Pedersen, R.B., Christie, D.M., and Miller, D.J. (Eds.)
Proceedings of the Ocean Drilling Program, Scientific Results Volume 187

1. Leg 187 Synthesis: Evolution of the Australian Antarctic Discordance, the Australian Antarctic Depth Anomaly, and the Indian/Pacific Mantle Isotopic Boundary[1]

David M. Christie,[2] Douglas G. Pyle,[3] Rolf B. Pedersen,[4] and D. Jay Miller[5]

ABSTRACT

Leg 187 of the Ocean Drilling Program set out to evaluate the geological history of the unique Indian-Pacific geochemical mantle domain boundary as it is recorded on the seafloor between its present location within the Australian Antarctic Discordance (AAD) and the southern continental margin of Australia. We used shipboard trace element analyses of basalt glasses, later confirmed and refined by onshore isotopic data, to locate this boundary within ±50 km through a grid of drill sites in seafloor of age 14–28 Ma. From these data, we infer that the Indian-Pacific mid-ocean-ridge basalt (MORB) mantle boundary is an intrinsic feature of the Australian-Antarctic Depth Anomaly (AADA), an anomalously deep region that spans the Southern Ocean Basin from the Australian to the Antarctic continental margins. For at least 25 m.y., the boundary has been located ~100 km east of the midline of the depth anomaly, between the –400 and –500 m depth anomaly contours. Pronounced westward deviations of the boundary along the present-day Southeast Indian Ridge (SEIR) and at ~20 Ma record transient westward propagation events of 3- to 4-m.y. duration. The origins of the distinct isotopic signatures that define the Indian and Pacific mantle provinces remain controversial, but it seems clear that a significant component of

[1]Christie, D.M., Pyle, D.G., Pedersen, R.B., and Miller, D.J., 2004. Leg 187 synthesis: evolution of the Australian Antarctic Discordance, the Australian Antarctic depth anomaly, and the Indian/Pacific mantle isotopic boundary. *In* Pedersen, R.B., Christie, D.M., and Miller, D.J. (Eds.), *Proc. ODP, Sci. Results,* 187, 1–41 [Online]. Available from World Wide Web: <http://www-odp.tamu.edu/publications/187_SR/VOLUME/SYNTH/SYNTH.PDF>. [Cited YYYY-MM-DD]
[2]College of Oceanic and Atmospheric Sciences, Oregon State University, 104 Ocean Administration Building, Corvallis OR 97331-5503, USA. dchristie@coas.oregonstate.edu
[3]SOEST, University of Hawaii, POST 612A, 1680 East-West Road, Honolulu HI 96822, USA.
[4]Department of Earth Science, University of Bergen, Allegaten 41, N-5007 Bergen, Norway.
[5]Integrated Ocean Drilling Program, Texas A&M University, 1000 Discovery Drive, College Station TX 77845-9547, USA.

Initial receipt: 3 December 2003
Acceptance: 1 June 2004
Web publication: 6 September 2004
Ms 187SR-201

the Indian mantle source was derived, as a by-product of the breakup of Gondwana, from ancient continental material that includes ancient accreted island-arc derived material.

The geochemical contrasts between lava populations from the Indian and Pacific domains have remained qualitatively constant through time. Basalts from the Indian domain are less evolved, with a smaller range of generally higher MgO contents than their Pacific counterparts. They are also more variable in other major and trace elements, consistent with derivation by generally smaller degrees of melting from a more variable melting regime. Quantitatively, however, the boundaries between the two groups have shifted, apparently reflecting a significant decrease in overall extents of melting. This shift, which occurred between ~14 Ma, the youngest age sampled during Leg 187, and ~7 Ma, the oldest age sampled by earlier dredging, most likely occurred when the northeastward absolute migration of the SEIR moved the spreading-axis segments that define the AAD into conjunction with the AADA and its underlying cooler mantle. In this cooler environment, overall extents of melting and magma supply rates were reduced, leading to the establishment of a predominantly extensional regime, characterized by extensive listric faulting within the AAD.

Leg 187, in combination with earlier dredge sampling of 0- to 7-Ma seafloor, also provided an unusual opportunity to evaluate post-eruptive geochemical and biological modification of seafloor lavas. Culturable microbes were isolated from lavas at all Leg 187 sites, strongly suggesting that significant microbial activity persists in the shallow ocean crust for at least 28 m.y. However, microbial forms that are commonly visible in electron microscopic images of alteration fronts and zeolite mineral surfaces associated with fractures in young volcanic glasses are no longer detectable in Leg 187 glasses. This implies that the locus of microbial activity has shifted away from pillow-rim volcanic glass to some other location within the samples, most likely to fractures within the more crystalline pillow basalts. This shift in the dominant mode of microbial activity may reflect a change from open-system seawater circulation to closed-system circulation due to burial. This change is consistent with patterns of alteration. On the one hand, isotopic studies of altered lavas indicate that of isotopic exchange with circulating seawater had ceased prior to 14 Ma, whereas on the other hand, mineralogical studies document ongoing alteration throughout the 14- to 28-Ma time span.

BACKGROUND

Australian Antarctic Discordance and Australian Antarctic Depth Anomaly

The Australian Antarctic Discordance (AAD) (Fig. F1) is a long-lived regional tectonic feature that encompasses the deepest (4–5 km) regions of the Southeast Indian Ridge (SEIR) and, indeed, the entire global mid-oceanic spreading system. Although the AAD has become well known for its anomalous depth, its defining characteristic is the unusual crenellated geometry formed by short (~100 km), deep axial valleys that are offset by long (2–300 km) transforms with alternating offset directions. This geometry has only developed during the past 25–30 m.y. (Vogt et al., 1983; Marks et al., 1999).

F1. Regional map of the Southeast Indian Ocean, p. 26.

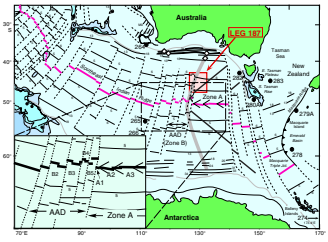

The present-day anomalously deep bathymetry of the AAD is the manifestation of the Australian Antarctic Depth Anomaly (AADA), a long-lived residual depth anomaly that extends from the Australian to the Antarctic continental margins and most likely predates the onset of continental rifting at ~100 Ma (Veevers, 1982; Mutter et al., 1985; Gurnis and Müller, 2003). North and south of the SEIR, the axis of the AADA describes a shallow arc that is convex to the west and cuts across the major eastern AAD fracture zones (Figs. F1, F2). The shape of this arc (Fig. F1) indicates a slow (~15 mm/yr) long-term eastward motion of the SEIR spreading system relative to a fixed north-south elongate mantle thermal anomaly (Marks et al., 1990, 1999; Gurnis et al., 1998; Ritzwoller et al., 2003). Initially, the AAD and the AADA were geographically distinct entities. The northeastward absolute motion of the plate boundary has systematically decreased their spatial separation through time, and they have come into conjunction only since ~12 Ma. These and other abbreviated terms are defined in Table T1.

The anomalous depth and segmentation of the AAD region are associated with unusually low magma production and with relatively cool upper mantle temperatures (e.g., Forsyth et al., 1987; Ritzwoller et al., 2003). East of the AAD, the SEIR in Zone A (Fig. F1) is characterized by a pronounced axial-ridge morphology with smooth off-axis topography, features that are typically associated with fast-spreading centers (>90 mm/yr). Within the AAD (Zone B), the SEIR is characterized by deep axial valleys with rough off-axis topography, features that are typically associated with slow-spreading centers (<50 mm/yr) (Palmer et al., 1993; Sempéré et al., 1991, 1996; West et al., 1994, 1997). In parts of the AAD, unusually large areas are dominated by chaotic seafloor terrain formed by listric faulting in a magma-poor, predominantly tectonic extensional environment (Christie et al., 1998). The contrasts in seafloor spreading between Zone A and the AAD are accompanied by distinct contrasts in the compositions and compositional diversity of basaltic lavas. These differences imply that a distinct change in fundamental seafloor accretionary processes occurs over a remarkably short distance along axis. Because it occurs at a uniform intermediate spreading rate of 74 mm/yr (DeMets et al., 1990), this change must reflect a fundamental change in magma supply (Palmer et al., 1993; Sempéré et al., 1991, 1996).

Origin of the Australian Antarctic Depth Anomaly

The AADA is a unique bathymetric feature that spans the Southern Ocean Basin from the Australian to the Antarctic continental margins. It is defined by seafloor depths that are as much as 1000 m deeper than surrounding (normal) seafloor of comparable age. The geodynamic process(es) that created and maintain the AADA have been active at least since seafloor spreading began at ~100 Ma and possibly for as long as 300 m.y. (Veevers, 1982; Mutter et al., 1985; Gurnis and Müller, 2003).

Gurnis et al. (1998) and Gurnis and Müller (2003) used plate reconstruction models to demonstrate that the inferred cold north-south elongate source of the depth anomaly coincides with the location, in a fixed-mantle reference frame, of a long-lived, pre-100-Ma western Pacific subduction zone. They argued that cold mantle beneath the AADA is associated with refractory subducted material from this subduction zone that accumulated at the 660-km mantle discontinuity. Mantle flow models based on this conclusion suggest that some of this refractory material with its associated mantle wedge material has recently been entrained into the upwelling upper mantle beneath the AAD.

F2. Satellite gravity map, p. 27.

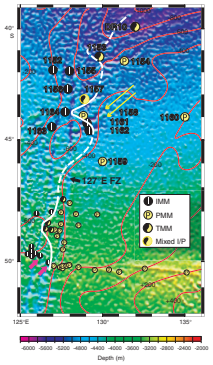

T1. Abbreviations and tectonic terminology, p. 40.

More recently, Ritzwoller et al. (2003) identified the Australian Antarctic Mantle Anomaly (AAMA), a northwest-southeast–trending linear band of high upper mantle seismic velocities that passes beneath the AAD. Northward migration of the SEIR over this oblique mantle anomaly would account for westward migration of the depth anomaly at a rate consistent with the curvature of the depth anomaly. They suggested that the AAMA consists of residual cold material that has risen to a level of neutral buoyancy in the upper mantle. The northwest-southeast orientation of the high-velocity AAMA appears, however, to be inconsistent with Gurnis's tectonic reconstruction. No mechanism has yet been proposed to account for either the persistence of cold, dense material at shallow mantle depths or the apparent 45° rotation of an original north-south–trending western Pacific paleosubduction zone.

The Indian/Pacific Mantle Isotopic Boundary

Background: Mantle Flow Hypotheses

Mid-ocean-ridge basalt (MORB) lavas erupted at Indian Ocean spreading centers are isotopically distinct from those of the Pacific Ocean, reflecting a fundamental difference in the composition of the underlying upper mantle (Subbarao and Hedge, 1973; Dupré and Allégre, 1983; Hart, 1984; Hamelin and Allégre, 1985; Hamelin et al., 1986; Price et al., 1986; Dosso et al., 1988; Mahoney et al., 1989, 1992). Along the SEIR, the Indian Ocean MORB mantle (IMM) isotopic province abuts the Pacific Ocean MORB mantle (PMM) province at a uniquely sharp boundary within the AAD. This was first recognized by Klein et al. (1988). Subsequent along-axis dredging (Moana Wave cruise MW88; Pyle et al., 1992) defined a very narrow (~50 km) zone within which lavas have transitional MORB mantle (TMM) isotopic signatures. This transition zone characterizes the present-day PMM/IMM boundary that exists beneath the western end of Segment B5 within the eastern AAD. Pyle et al. (1992) also recovered IMM lavas from two off-axis (3–4 Ma) sites located on flow lines directly south of sections of the B5 axis that presently erupt TMM and PMM lavas. The simplest explanation for this change in mantle source beneath Segment B5 is a recent westward migration of PMM during the last 4 m.y. at ~25 mm/yr (Pyle et al., 1992).

The apparent migration rate of the isotope boundary across Segment B5 (~25 mm/yr) is intermediate between the rate of westward migration of the AADA (~15 mm/yr) and rates of rift propagation toward the AAD from the east (30–40 mm/yr). These faster rates are consistent with hypotheses of Alvarez (1982, 1990) that invoke large-scale upper mantle flow from the shrinking Pacific to the expanding Indian Ocean Basin as Australia separated from Antarctica. If such a flow was initiated 30–40 m.y. ago upon final continental separation of the South Tasman Rise from Antarctica (Hinz et al., 1990), migration velocities of ~40 mm/yr would be required to account for the recent arrival of PMM beneath the eastern margin of the AAD. The IMM/PMM boundary configuration produced by this type of migration is indicated by the heavy black lines in Figure F1.

Pyle et al. (1995) set out to evaluate the Alvarez rapid migration hypothesis through a regional geochemical study based on basalts from Deep Sea Drilling Project (DSDP) Legs 28 and 29. At the same time Lanyon et al. (1995) studied altered basalts from four dredge sites close to the continent/ocean boundary north of the AAD. Both studies

showed that IMM was present east of the AAD prior to 30 Ma, apparently consistent with large-scale upper mantle flow from the east. However, because of the sparse and nonideal distribution of available samples, it was not possible to conclusively distinguish between possible off-axis boundary configurations consistent with rapid migration and a boundary that was permanently associated with the AADA.

To better locate the Indian/Pacific mantle boundary off axis, the Boomerang 05 (BMRG05) and Sojourn 05 (SOJN05) expeditions of the *Melville* mapped and sampled 3- to 7-Ma seafloor in Segment B5 and the adjacent Segments A1 and B4. Christie et al. (1998) showed that the eastern limit of the IMM domain coincides with a west-pointing, V-shaped topographic boundary that separates chaotic terrain to the west from normal seafloor. The geometry of this remarkable boundary is consistent with the ~25 mm/yr westward migration of the PMM/IMM boundary across Segment B5 during the last ~4 m.y. (Fig. F2). Off-axis dredging east of the AAD recovered PMM lavas from seafloor as old as ~7 Ma. This inability to locate the PMM/IMM boundary in Zone A left the two principal mantle migration hypotheses unresolved. The question of whether the topographic and isotopic boundary within Segment B5 represented the culmination of long-term, rapid migration or a localized perturbation in a boundary associated in the long term with the AADA remained unresolved.

Leg 187: Resolving the History of the Mantle Boundary

The principal objective of Ocean Drilling Program (ODP) Leg 187 was to evaluate the long-term (10–30 Ma) history of this mantle domain boundary, focusing on the two alternate hypotheses outlined above: (1) that the recent migration is the culmination of long-term, rapid migration of PMM from the east or (2) that the IMM/PMM boundary is an intrinsic feature of the AADA. To be consistent with the second hypothesis, the 0- to 4-Ma migration must represent a localized short-term perturbation of a stable long-term boundary location (Pyle et al., 1992; Christie et al., 1998; Christie, Pedersen, Miller, et al., 2001).

LEG 187 OBJECTIVES AND IMPLEMENTATION

Locating the Isotopic Boundary

The success of Leg 187 depended on our ability to locate the Indian/Pacific mantle isotopic boundary through its expression in the geochemistry of MORB lavas from 14- to 28-Ma seafloor north of the AAD. Because the isotopic analyses required to define the IMM/PMM boundary cannot be performed at sea, we employed diagnostic elemental analyses as a proxy to distinguish IMM, PMM, and transitional lava compositions using inductively coupled plasma–atomic emission spectrometry (ICP-AES)—the first such analyses performed during an ODP cruise. At critical times during the leg, onboard analyses were completed within 12 hr of core recovery to optimize selection of the next drilling target and ensure optimal coverage of the boundary trace.

Based on existing data for 0- to 7-Ma dredge samples collected from the AAD prior to Leg 187 (Pyle et al., 1992, 1995; D. Pyle, unpubl. data, 2004), we were able to identify two discrimination diagrams, Ba vs. Zr/Ba and MgO vs. Na_2O/TiO_2, that were within the onboard analytical capabilities of the *JOIDES Resolution* and could reliably assign >95% of ex-

isting axis and near-axis dredge samples to their correct, isotopically defined mantle source type. For reliability, these analyses must be performed on fresh basaltic glass fragments, as whole-rock samples are subject to chemical alteration, especially for Ba. In order to obtain reliable Ba and Zr data from small basaltic glass samples, it was essential to accelerate the planned installation of the ICP-AES instrument aboard the *JOIDES Resolution*. Although the instrument was not installed until immediately prior to our departure, we were able to develop analytical protocols and obtain satisfactory analytical performance throughout the leg. The onboard Zr/Ba data enabled us to assign a source affinity at most sites. Of the 13 sites drilled, 8 were correctly (as determined by later isotopic analysis) assigned to a PMM, TMM, or IMM source. Glasses from four sites were designated onboard as "Transitional Pacific" and subsequently proved to be of IMM affinity. One lava from Site 1164 that plotted just inside the PMM boundary (on the Zr/Ba graph shown in Fig. F8) proved subsequently to be of IMM affinity, leading to a "mixed" designation for that site in the Leg 187 *Initial Reports* volume (Christie, Pedersen, Miller, et al., 2001). Na_2O/TiO_2 data were not immediately useful on board, as Leg 187 samples have systematically lower Na_2O than their younger (dredged) counterparts. In retrospect, Na_2O/TiO_2 ratios appear to be reliable source indicators for the Leg 187 data alone; the PMM/IMM boundary is well defined at lower Na_2O/TiO_2 values than for the near-zero–age samples.

A Responsive Drilling Strategy

In order to locate the Indian/Pacific mantle isotopic boundary as precisely as possible over as long a seafloor age interval as possible, our drilling strategy had two key elements. The first was to maximize the number of sites drilled, limiting penetration depth into basaltic basement to a nominal objective of 50 m. Even this limited penetration was achieved at only five sites due to poor drilling conditions in broken pillow flows and talus. The second element of our strategy was one of responsive site selection (from a slate of 19 preapproved sites) based on rapid chemical analysis within 24 hr of sample recovery. At key decision points throughout the leg, we reviewed and modified our drilling strategy on the basis of shipboard geochemical analyses of newly recovered basalt glasses.

Selection of the initial suite of approved potential drill sites was complicated by the absence of measurable sediment cover across much of the region. The paucity of sediment most likely reflects winnowing by strong bottom currents associated with the Circum-Antarctic Current as it crosses the SEIR through the deep AAD. Drillable sites were selected on localized sediment pockets detected by single-channel seismic imaging during the site survey cruises, Boomerang 5 (BMRG05) and Sojourn 5 (SJRN05) of the *Melville*. Three additional sites were surveyed by the *JOIDES Resolution* during the transit from Site 1158 to Site 1159; two of these were drilled as Sites 1161 and 1162. Because we expected sediments across the region to be reworked and of little use for stratigraphy and because we needed to maximize the number of sites drilled, we chose to wash through the sediment sections. Wash cores covering significant sediment intervals at 10 sites were described on board but have not been studied further.

Subsurface Biosphere

An investigation of the nature and geological impacts of microbial life on and beneath the ocean floor was an important goal of Leg 187. Much attention has been focused on the nature of microbes that live on and contribute to the alteration of oceanic basalts, especially the glassy rims of pillow lavas (Thorseth et al., 1995; Furnes et al., 1996; Fisk et al., 1998; Torsvik et al., 1998). This phenomenon has been documented from Iceland (Thorseth et al., 1991), ODP Hole 896A at the Costa Rica Rift, and the Arctic regions of the Mid-Atlantic Ridge (Thorseth et al., 1999). During Leg 187, considerable effort was made to obtain rock, sediment, and water samples with minimal contamination from the shipboard environment for onshore deoxyribonucleic acid (DNA) analysis of cultured and uncultured materials. A large suite of altered basaltic samples was also collected to enable an electron and optical microscopic search for evidence of microbial activity.

Uncontaminated rock and sediment samples collected during Leg 187 yielded a variety of viable microbial cultures. **Lysnes et al.** (this volume) performed extensive DNA sequence analysis of material extracted from basalt samples and compared the results with control samples of sediment, drilling mud, and seawater. They also performed extensive culture experiments designed to enhance the growth of microbial populations from basalt samples.

Lysnes et al. showed that the basalt samples contain diverse microbial populations that are distinct from those of Leg 187 sediment samples and from local seawater. Only a relatively small subset of the native basalt population grew successfully in the various enrichment cultures. The native basalt populations and the enrichment cultures were both dominated by gamma *Proteobacteria*, with five clusters of closely related microbes responding to the culture media. Additional microbes that responded well to the culture media clustered within the CFB (*Cytophaga*/*Flavobacterium*/*Bacteroides*) and *Bacillus*/*Clostridium* groups.

The existence of culturable microbes in Leg 187 samples strongly suggests that there is significant microbial activity in shallow ocean crust as old as 28 Ma. However, neither conventional nor scanning electron microscopic examination revealed any evidence of microbial morphologies in alteration zones abutting fresh volcanic glass from any Leg 187 site (Thorseth et al., 2003). This absence of morphological evidence contrasts with parallel studies of 0- to 2-Ma dredge samples from the AAD, which revealed several morphological microbial forms associated with similar alteration fronts and with zeolite mineral surfaces within fractures in the glass. This suggests that microbial activity ceased along the glass front between 2 and 14 Ma. After this time, microbial activity continued (or possibly relocated) elsewhere within the samples, most likely in fractures within the pillow basalts. This shift in the dominant mode of microbial activity may coincide with the cessation of active seawater circulation due to burial, perhaps reflecting a change in pore fluid chemistry at this time. Such a change may also have led to an observed change in the style of chemical alteration at the glass front (see **"Mineralogical and Chemical Aging of Basalts,"** p. 8, in "Alteration Studies").

ALTERATION STUDIES

Leg 187 was unusual in the large number of holes (23 holes at 13 sites) drilled into basaltic basement and the wide range of crustal ages sampled. The array of drilled sites approximates three ~14- to 28-Ma flow lines that encompass the known contrasts in morphology and geochemical diversity along the SEIR. When combined with the existing suite of young (0–7 Ma), well-characterized dredge samples, these samples provide a rare opportunity to document the progressive alteration (weathering) of seafloor basalts as they age and move away from the spreading axis.

No evidence for pervasive hydrothermal alteration of basalts was encountered during Leg 187.

Microbial Alteration Studies

Thorseth et al. (2003) used conventional microscopy and scanning electron microprobe (SEM) to investigate the mineralogy of glass alteration and the role of microbes in this alteration, using both Leg 187 core material and glasses from dredge samples of younger (0–2.5 Ma) seafloor.

For 0- to 2.5-Ma samples from the AAD, there is ample evidence of ongoing microbial activity along fracture surfaces in the basalt glass and on zeolite crystal surfaces within hairline fractures. Alteration halos on glasses from Leg 187 cores are much thicker adjacent to fractures, but glassy rim thicknesses do not change significantly with age. Microbial morphologies are rare within these glassy rims, although some Mn-rich spherical forms, interpreted as having a microbial origin, were detected in more porous regions within altered glass and in some fractures. At least one style of diffuse, irregular alteration front that is present only in the Leg 187 glasses is inferred to have formed postburial and in the absence of microbial activity (Fig. F3).

Mineralogical and Chemical Aging of Basalts

Miller and Kelley (this volume) examined the mineralogy and major and trace element chemistry of altered (discolored) basalt whole-rock samples from all 13 Leg 187 sites. They found a uniform and ubiquitous suite of alteration products dominated by Fe oxyhydroxides, smectite-group clays, and palagonite. The alteration assemblages occur in one of four modes: (1) as replacements of irregular patches in the groundmass, (2) as partial or complete replacements of phenocrysts, (3) as vesicle linings and fillings, or (4) as vein or fracture linings and infill. These modes occur in varying combinations in different samples. At Site 1162, some breccia clasts contained high-temperature greenschist facies alteration assemblages that include talc, actinolite, chlorite, and albite.

The dominant chemical indicators of alteration appear to be decreased MgO and increased loss on ignition; for both these indicators, the maximum values at a given site increase systematically with secondary mineral abundance. Both indicators also increase with distance off axis over most of the drill sites, with the notable exception of the oldest three sites, 1152, 1153, and 1154 (25–28 Ma), which are visually and chemically less altered than the younger sites, 1155, 1156, and 1157 (20–25 Ma) (Fig. F4). In three composite flows at Site 1160, we documented pervasive MgO loss from pillow interiors, relative both to

F3. Zeolite veins, p. 28

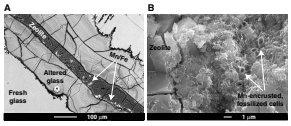

F4. "Isocon plots" showing inter-element alteration relationships, p. 29.

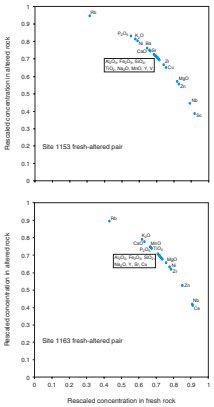

their glassy margins and to the underlying massive potions of the composite flows (see Shipboard Scientific Party, 2001). A systematic onshore analysis of alteration chemistry further reveals that, relative to Al_2O_3, which appears to have been immobile, MgO, Fe_2O_3 (total), MnO, and SiO_2 are lost from altered samples, whereas CaO and K_2O are added during the alteration process (**Miller and Kelley,** this volume).

S. Krolikowska-Ciaglo and F. Hauff (pers. comm., 2003) compared trace element and isotopic compositions of discolored, visibly weathered outer surfaces of basalt pieces with their less altered interiors and, where possible, with coexisting fresh glass. They report a chemical alteration signature that is uniform in nature and extent across the range of depth and latitude encompassed by the drilling. This behavior contrasts with that of the major elements as reported by **Miller and Kelley** (this volume) and suggests a contrary conclusion—that chemical exchange with seawater had ceased or at least slowed significantly prior to the ~14-Ma age of the youngest Leg 187 site. Krolikowska-Ciaglo and Hauff report that alteration is characterized by loss of MgO (in agreement with Miller and Kelley and onboard studies) and by pervasive addition of boron plus the high field–strength cations Cs, Rb, U, and K. Concentrations of these added elements correlate well with one another and with visual estimates of the degree of alteration. Predictably, Nd contents and $^{143}Nd/^{144}Nd$ isotopic ratios are not affected by alteration. Sr content does not increase with degree of alteration, but isotopic exchange with seawater increased $^{87}Sr/^{86}Sr$ significantly, with the most altered samples tending to have the most radiogenic Sr (Fig. **F5**). Krolikowska-Ciaglo and Hauff postulate that this exchange occurs primarily at sites within the interlayers of hydrated smectites produced by the alteration process.

Within individual drill holes, $^{207}Pb/^{204}Pb$ and $^{208}Pb/^{204}Pb$ ratios remain constant while $^{206}Pb/^{204}Pb$ ratios increase with the degree of alteration. From fresh glass values of 6–8, similar to upper mantle values, $^{238}U/^{204}Pb$ (μ) values range up to a maximum of 183 in altered basalts as a result of secondary addition of seawater uranium. This uranium enrichment leads to significant radiogenic ingrowth of ^{206}Pb that, with time, shifts altered basalts along horizontal arrays in correlation diagrams of $^{206}Pb/^{204}Pb$ vs. both $^{208}Pb/^{204}Pb$ and $^{207}Pb/^{204}Pb$ (Fig. **F6**).

Regional Alteration Patterns

None of the alteration studies indicate any difference in alteration style between Zone A and the AAD or between Indian- and Pacific-type lavas. This is, perhaps, not surprising from the viewpoint of geochemistry because the differences between Indian and Pacific types are subtle and confined for the most part to isotopic and trace element compositions. Of more interest is the implication that seafloor topographic style had no effect on alteration style. The contrast between the chaotic, predominantly extensional terrain of Zone B and the dominantly magmatic abyssal-hill terrain of Zone A (Christie et al., 1998) should be reflected in structure, porosity, and permeability as well as in the nature and distribution of high- and low-temperature seawater circulation, so the absence of discernible alteration effects is surprising. An alternate interpretation is that the topographic contrast within the AAD is stronger at present than it was during the 14- to 28-Ma period.

In terms of the alteration process itself, interesting contrasts have emerged between alteration-related studies that indicate no significant

F5. $^{143}Nd/^{144}Nd$ vs. $^{87}Sr/^{86}Sr$ isotopic compositions, p. 30.

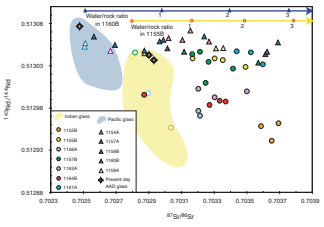

F6. $^{208}Pb/^{204}Pb$ vs. $^{206}Pb/^{204}Pb$ isotopic compositions of altered samples, p. 31

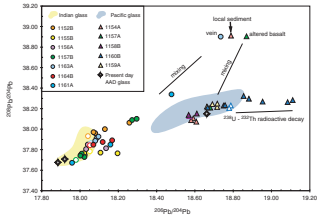

changes from 14 to 28 Ma and those that do record change. In the former category, Thorseth et al. (2003) reported that microbial activity and much of the mineralogical alteration of basaltic glass appears to have terminated before the 14-Ma age of the youngest drilled samples. A particular style of "granular alteration" of glass appears only to develop postburial and to be unrelated to microbial activity. S. Krolikowska-Ciaglo et al. (pers. comm., 2003) reported that isotopic and trace element exchange with seawater also effectively ceased before 14 Ma. In contrast, **Shau et al.** (this volume; see **"Magnetic Properties,"** below) report that natural remanent magnetization (NRM) values for drilled basalts decrease progressively with increasing age and **Miller and Kelley** (this volume) report ongoing mineralogical and chemical evolution of altered basaltic rock (but not glass) samples. One possible explanation for these disparate observations is that seawater circulation had effectively ceased by 14 Ma. This would allow for chemical equilibrium to be established in terms of trace element exchange and in the processes of glass alteration, especially in those processes mediated or enhanced by microbial activity. It is a common observation in altered MORB samples that fresh glass fragments can be isolated by clay-rich alteration products and preserved for many millions of years. Perhaps the chemical gradients that lead to reaction at the active inner edges of the alteration rims can only be maintained while there is active circulation and alteration ceases once flow stagnates. In contrast, (partially) crystalline basalts appear to be thoroughly permeated by seawater and may take much longer to reach equilibrium once circulation ceases. These processes may also depend on diffusive or other low-level flow that continues as burial proceeds and after fracture permeability has closed. Ongoing mineralogical changes are also required to explain the progressive loss of magnetic remanence as the lavas age.

The reasons for the inferred cessation of crustal seawater circulation in this area are of interest because of the general absence of sediment cover (Christie, Pedersen, Miller, et al., 2001). Despite the apparent absence of sediment, our early attempts to dredge from seafloor older than ~7 Ma failed to recover rock samples but frequently recovered Fe-Mn oxide crusts. We speculate that the older seafloor in the region is sealed by such crusts.

MAGNETIC PROPERTIES

Shau et al. (this volume) determined the magnetic properties and oxide mineralogy of a large suite of samples. The dominant magnetic carrier in pillow basalts is maghemite, presumed to have formed by low-temperature oxidation of primary titanomagnetite. A significant proportion of the magnetized material is in the form of small (<0.5 µm) single-domain Fe-Ti oxide grains within interstitial glass. NRM values are typical for MORB and decrease with increasing age across the 14- to 28-Ma interval spanned by the Leg 187 sites. This evidence for ongoing alteration contrasts with that of S. Krolikowska-Ciaglo et al. (pers. comm., 2003) (see **"Regional Alteration Patterns,"** p. 9, in "Alteration Studies"), who concluded that low-temperature alteration of pillow basalts was essentially complete by 14 Ma.

In the massive basalts of Hole 1160B, which are less altered than coexisting pillow basalts (Christie, Pedersen, Miller, et al., 2001), the dominant magnetic carrier is primary titanomagnetite, which occurs as homogeneous grains a few tens of micrometers in size. In the single

greenschist-facies metadiabase clast from Hole 1162C, the dominant carrier is magnetite, formed by hydrothermal alteration of primary subhedral titanomagnetite grains as large as a few hundred micrometers.

The magnetic characteristics of pillow basalt samples do not change from east to west across the region, indicating that these properties are insensitive to mantle source signature and topographic style, as discussed in the preceding section. Noting that aeromagnetic anomaly amplitudes (Vogt et al., 1983) are lower within the AAD than in Zone A, **Shau et al.** (this volume) point out that the magnetic uniformity of the pillow basalts across the region requires a significant contribution from the lower crust to the total magnetic field. This observation is consistent with the extensive exposures of Layer 3 and Layer 4 materials at the seafloor that can be inferred from the association of chaotic terrain with extensive megamullions in Segments B4 and B3 (Christie et al., 1998).

GEOCHEMISTRY AND PETROLOGY

Defining the Mantle Domains

Lead Isotopic Signatures

Pyle et al. (1992) showed that the near-zero–age IMM and PMM lavas define discrete fields in any of several binary combinations of the isotopes of Sr, Nd, and Pb. Relative to PMM lavas, IMM lavas have higher $^{87}Sr/^{86}Sr$ and lower $^{206}Pb/^{204}Pb$, $^{207}Pb/^{204}Pb$, and $^{208}Pb/^{204}Pb$. More recently, Pearce et al. (1999), Hanan et al. (2000a, 2000b, submitted [**N1**]), and Kempton et al. (2002) have shown that binary plots of Hf and Nd isotopic ratios can also offer an effective IMM–PMM discriminant, with IMM lavas having higher $^{176}Hf/^{177}Hf$ and lower $^{143}Nd/^{144}Nd$ than their PMM counterparts. Here we have chosen to use Pb isotope variations, primarily $^{206}Pb/^{204}Pb$, of fresh basaltic glass samples as our definitive discriminant of IMM–PMM sources in keeping with our previous work on the near-axis and axial SEIR data set (Pyle et al., 1992, 2000) (Fig. **F7**).

Pb isotope ratios for selected Leg 187 glass samples were analyzed by thermal ionization mass spectrometry (TIMS) at San Diego State University (California) in collaboration with B. Hanan and at the University of Hawaii by D. Pyle (Pyle et al., 2000; D. Pyle, pers. comm., 2004). These data are complemented by a comprehensive suite of whole-rock and glass Sr and Nd isotope ratios (**Pedersen et al.,** this volume) and by a suite of predominantly whole-rock Hf, Pb, Nd, and Sr isotope ratios (Kempton et al., 2002). To classify the Leg 187 and other off-axis samples, we use IMM and PMM fields based on an updated compilation of near-zero–age dredge data (Fig. **F7**). A few zero-age samples from the isotopic boundary zone in Segment B5 plot between the IMM and PMM fields and define a TMM domain. TMM lava compositions are consistent with their derivation from a mixture of IMM and PMM source components. Several samples that we now define as TMM were designated as TPMM (for Transitional Pacific MORB mantle) during Leg 187 (Christie, Pedersen, Miller, et al., 2001), and this term was subsequently used by Kempton et al. (2002). We no longer include "Pacific" as a modifier for transitional lavas, as TMM defines a continuum between PMM and IMM.

Our Ba-Zr–based shipboard source designations (reported by Christie, Pedersen, Miller, et al., 2001) compare well to our (definitive) classifica-

F7. $^{208}Pb/^{204}Pb$ vs. $^{206}Pb/^{204}Pb$ of fresh basaltic glasses, p. 32.

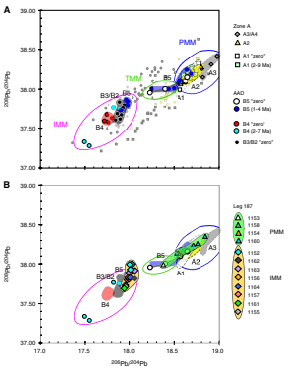

tion based on later shore-based isotopic determinations. The isotopic data confirm that we correctly located the Indian/Pacific boundary during Leg 187 using our Ba vs. Zr/Ba proxy (Fig. F8), despite minor differences between the Leg 187 and zero-age compositional fields. For several samples that plot close to the field boundaries or in a low-Zr/Ba extension of the Pacific field, we used an onboard TPMM designation. These included IMM lavas from Sites 1152, 1155, and 1162 and one PMM lava from Site 1158. A single IMM sample from Site 1164 was designated PMM. Although these sample designations led us to classify some sites ambiguously as transitional or mixed, no IMM site was misidentified as PMM or vice versa. The isotopic data resolve these ambiguities and greatly improve the resolution of the boundary (Figs. F2, F8).

Several sites that yielded either TMM lavas or lavas of more than one type (mixed sites) are of particular importance for our interpretation of the Indian/Pacific boundary configuration. They include the following.

F8. Ba vs. Zr/Ba plot used as a discrimination proxy during Leg 187, p. 33.

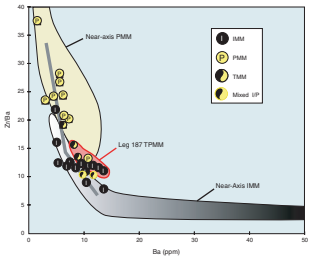

Site 1157

Site 1157 is mixed IMM/PMM. This is the only Leg 187 site to include both IMM and PMM lavas. A single glass from a core catcher of Hole 1157A is IMM according to both Pb and Hf-Nd isotopic data, but three shallower whole-rock samples from this hole are PMM (Kempton et al., 2002). Three whole-rock samples from Hole 1157B, ~200 m away, are IMM. Hole 1157B extends to greater depth through more intact pillow basalts than Hole 1157A, which returned only rubble interpreted as erosional in origin. Although stratigraphic sequences cannot be reliably inferred from drilled rubble, it is probable that PMM lavas overlie IMM at this site.

Site 1158

Site 1158 is mixed TMM/PMM. A single whole-rock sample from Hole 1158A lies well within the IMM field for Hf-Nd isotopic ratios and was classified as IMM by Kempton et al. (2002) (see **"Hf Isotopic Signatures,"** p. 14), but its $^{206}Pb/^{204}Pb$ and $^{208}Pb/^{204}Pb$ ratios place it within the standard TMM field (Fig. F7), although it has unusually high $^{207}Pb/^{204}Pb$. A glass sample and a basalt whole rock from Hole 1158B and a diabase from Hole 1158C are clearly PMM. Hole 1158A, which is 270 m and 440 m south of Holes 1158B and 1158C, respectively, intersected basement at 70–80 m greater depth below the seafloor, in this case suggesting that PMM lavas may overlie TMM lavas.

Site 1153

All analyzed samples from this site plot within a TMM field that lies between the IMM and PMM fields similar to present-day TMM lavas from Segment B5 west (Pyle et al., 1992).

DR 10

Dredge 10 of Lanyon et al. (1995) lies slightly north of Sites 1153 and 1154 (Fig. F2) and was considered by those authors to be of Indian affinity. Although accurate age corrections are difficult to determine for these samples, by our current classification, lavas from this dredge are from a TMM source.

We interpret these four sites as lying within the Indian/Pacific isotope boundary zone. At zero age, the transition zone defined by the occurrence of TMM lavas extends <50 km along axis (Pyle et al., 1992) and it seems reasonable to interpret the presence of TMM lavas at Sites 1153 and 1158 and in DR 10 as defining a boundary zone of similar width. At Site 1158, PMM lavas occur only ~50 km east of the 127°E Fracture Zone

(Fig. F2), and this distance may define the maximum width of the transition zone at this latitude. The alternation of PMM, TMM, and IMM lavas along a generally north-south transect through Zone A west; the anomalous occurrence of PMM and TMM lavas to the west of IMM lavas across the closely spaced Sites 1158, 1161, and 1162; and, especially, the probable emplacement of PMM lavas over TMM or IMM lavas at these sites all require that the mantle sources for both lava types exist in close proximity and that these distinct magmas are effectively isolated en route to the surface. We interpret these observations as resulting from a short-lived westward propagation event, comparable to the recent migration of the Indian/Pacific boundary across Segment B5. This interpretation is supported by a pair of distinctive oblique seafloor lineaments that pass close to the sites (Marks et al., 1999) (Fig. F2) and coincide roughly with the location of a propagating rift inferred from aeromagnetic data by Vogt et al. (1983).

Sr and Nd Isotopic Signatures

Pedersen et al. (this volume) focused on the Sr-Nd isotope systematics of Leg 187 glasses and especially on their spatial variability. They showed that Leg 187 isotopic data define two spatially separated intersecting linear trends in Sr-Nd and Pb-Hf isotope plots. In their Nd-Sr binary isotopic diagram (Fig. F9, lower panel), glasses from sites in Zone B, west of the 127°E Fracture Zone, plot along a well-defined negative western trend. Glasses from sites east of the 127°E Fracture Zone form a flat eastern trend with relatively invariant $^{143}Nd/^{144}Nd$. Similar intersecting linear trends can also be discerned in the Pb-Pb isotopic binary plots discussed above (Fig. F7). The locations of individual sites or samples along these trends appear to be related to distance from the 127°E Fracture Zone and/or the depth anomaly (Pedersen et al., this volume). The development of paired linear trends suggests an unusual scenario in which both PMM and IMM end-members have mixed with a third, intermediate boundary end-member, but not with each other. The situation appears to have persisted during the time span represented by Leg 187 basalts, but not until the present.

The eastern (PMM) and western (IMM) end-member compositions lie within the much broader overall PMM and IMM compositional ranges. They are most strongly expressed at Sites 1160 and 1152, which are, respectively, the easternmost and westernmost Leg 187 sites in terms of their distance from the 127°E Fracture Zone. In Nd-Sr and Hf-Pb isotopic space, the intermediate end-member appears to be most strongly expressed at Site 1162 (Fig. F9). Site 1161, which consistently plots at the intersection of the eastern and western trends, is also strongly influenced by this end-member. Site 1157 lavas plot close to the intersection and along both trends, consistent with the mixed source affinities of lavas at this site (see "Lead Isotopic Signatures," p. 11, above). Because both these sites lie close to the Indian/Pacific mantle boundary, Pedersen et al. (this volume) refer to the intermediate end-member as the "boundary component."

Mixing relationships similar to those described by Pedersen et al. (this volume) as the eastern trend were recognized by Kempton et al. (2002) (see "Hf Isotopic Signatures," p. 14), who showed that IMM lavas from Leg 187 sites in Zone A west have generally higher εHf and εNd values than those from other Leg 187 sites (Fig. F10). Because the paired compositional arrays are discernible only in the Leg 187 data set and the boundary component appears to be restricted to Zone A west,

F9. εNd vs. $^{206}Pb/^{204}Pb$ and $^{87}Sr/^{86}Sr$ basaltic glasses, p. 34.

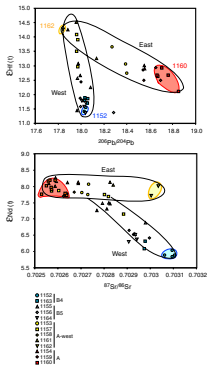

F10. εHf vs. εNd diagram for AAD region, p. 35

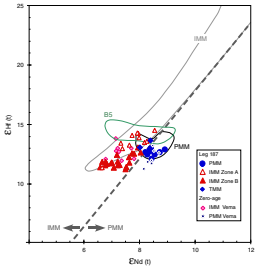

the three-component mixing that they represent was a localized and transient phenomenon that likely terminated at ~12–15 Ma, as northeast migration of the SEIR moved the 127°E Transform from west to east, first across the sublithospheric mantle locus of the depth anomaly and, 1–2 m.y. later, across the Indian/Pacific mantle boundary (see fig. 4 in Marks et al., 1999).

Hf Isotopic Signatures

Kempton et al. (2002) reported an extensive suite of new Nd, Pb, and Hf isotopic data for basaltic whole-rock and glass samples from Leg 187, supplemented by near-zero–age samples from the 1976 Vema dredges reported by Klein et al. (1988). Although there is almost complete overlap in the fields of published $^{176}Hf/^{177}Hf$ data from the Pacific and Indian Oceans, basalts derived from IMM and PMM sources in the AAD and Zone A can be effectively discriminated using Nd and Hf isotope systematics. Relative to PMM, the IMM field is systematically displaced to lower $^{143}Nd/^{144}Nd$ for a given $^{176}Hf/^{177}Hf$ value. Kempton et al. (2002) defined a linear discriminant separating PMM from IMM in εNd-Hf isotopic space (Fig. **F10**) and used this guideline to assign each Leg 187 drill site to a mantle isotopic domain. Newly available Hf isotope analyses of a much larger suite of near-zero–age dredged glasses (Hanan et al., 2000a, 2000b, submitted [**N1**]) generally confirm the validity of this discriminant, although three Segment A1 (PMM) dredges plot within the IMM field.

The Hf-Nd source assignments of Kempton et al. (2002) differ from the standard (Pb isotope) assignments at only two Leg 187 sites. As with the shipboard assignments, the differences are minor and have no effect on the inferred location of the Indian/Pacific mantle boundary. Sites for which the Hf isotopic designation differs from the standard are discussed briefly below.

Site 1153

Site 1153 is mixed IMM/PMM. These basalts are designated as transitional (TPMM) by Kempton et al. (2002) because the two analyzed samples are close to, but on opposite sides of, the discriminant boundary (Fig. **F10**).

Site 1158

Site 1158 is PMM/IMM. A whole-rock sample from Hole 1158A lies well within the IMM field for Hf-Nd isotopic ratios. Our standard designation based on Pb isotopic ratios is TMM, although it has high $^{207}Pb/^{204}Pb$ relative to other TMM samples. This is the only sample for which the two isotopic systems differ in their source designation. All other samples from this site are unequivocally PMM.

Kempton et al. (2002) recognized the importance of Zone A west lavas as a local end-member consistent with the **Pedersen et al.** (this volume) definition of the boundary component (see **"Sr and Nd Isotopic Signatures,"** p. 13). IMM lavas from Zone A west have relatively high εHf and high εNd relative to all other Leg 187 sites (Fig. **F10**). Within the Kempton et al. data set, Zone A west lavas have higher εHf than most AAD and Zone A lavas overall, but additional data from Hanan et al. (2000a, 2000b, submitted [**N1**]) (Figs. **F10, F13**) extend the overall IMM field to higher values than those of the Zone A west Leg 187 sites. This observation has important implications for interpretations of the geodynamic origin of the AAD and the depth anomaly (see **"Geochem-**

ical Evidence for Entrainment," p. 19, in "Constraints on the Origin of the ADD and the AADA" in "Dynamics and Origin of the AAD").

Location of the Indian/Pacific Isotopic Domain Boundary

Perhaps the most remarkable aspect of the Leg 187 isotope systematics is the consistency of interpretation over the entire region and the absence of significant discrepancies. The isotopic data discussed in the preceding sections enable us to locate the off-axis trace of the isotopic boundary with remarkable precision, within <50 km, over much of the last ~25 m.y. Between the SEIR (~50°S) and 43°S, the boundary trace shown in Figure F2 is drawn to pass to the east of the easternmost IMM sites and west of the westernmost PMM and TMM sites. The boundary is located ~100 km east of the axis (midline) of the depth anomaly, between the –400- and –500-m depth anomaly contours. A pronounced westward deviation of the boundary trace required by the presence of PMM lavas at Sites 1158 and 1157 is interpreted as recording a transient westward propagation event very similar in scale and duration to the well-documented recent (3–4 Ma) propagation of a PMM source into a preexisting IMM source region beneath Segment B5. North of 42°S (>26 Ma), the depth anomaly broadens and deepens, sample density is sparse, and the boundary is poorly constrained. The presence of TMM lavas at Site 1153 and in DR 10 suggests that the boundary passes close to these sites, rather than turning to the east with the depth anomaly contours.

Variations in the Melting Regime

Olivine Compositions and the Origins of Indian- and Pacific-Type MORB

Sato (this volume) undertook a thorough study of mineral compositions for a suite of Leg 187 basalt samples. He identified a group of primitive basalts that can reasonably be assumed to have evolved from their primary compositions by crystal fractionation of olivine alone. For each of these samples, he used an olivine addition calculation to estimate a primary magma composition that would be in equilibrium with mantle olivine. These equilibrium mantle olivine compositions can, in turn, be used to estimate the depth at which the primary magma last equilibrated with mantle material.

Primary Pacific-type MORB compositions determined in this way are derived from greater depths (15 kbar and 45 km) than primary Indian-type MORB compositions (10 kbar and 30 km). Consequently, even the most primitive Pacific-type lavas must have undergone more fractionation prior to eruption than their Indian-type counterparts. This conclusion is consistent with the presence of cooler mantle beneath the AAD.

Major and Trace Element Constraints

A remarkable and unexpected outcome of Leg 187 is the observation that near-axis (0–7 Ma) IMM lavas differ from their Leg 187 counterparts in important aspects of their trace and major element compositions. Many of these differences are in parameters that are most strongly influenced by depth and extent of melting (C.J. Russo et al.,

pers. comm., 2004), but differences in source composition are also apparent.

As a group, the IMM lava population is distinct from the PMM group in having significantly more variable major, minor, and trace element contents at a given MgO content. IMM lavas are characterized by lower FeO, CaO, and TiO_2 and higher K_2O, Al_2O_3, Na_2O, and SiO_2 than PMM lavas, suggesting a wider and more variable range of primary compositions (Fig. **F11A**) (Pyle, 1994; C.J. Russo et al., pers. comm. 2004). PMM lava compositions are relatively invariant at a given MgO content and the near-axis PMM population extends over a broader range to significantly lower MgO values, suggesting a dominant control by crystal fractionation processes, but this distinction is barely apparent in the Leg 187 samples.

One key compositional difference consistent with the derivation of IMM magmas by lower extents of melting from shallower depths in a cooler mantle regime is expressed in fractionation-corrected Na_2O and FeO contents, expressed as Na8 and Fe8 (Klein and Langmuir, 1987). Near-axis (0–7 Ma) IMM lavas have distinctly higher Na8 and lower Fe8 values than all other AAD and Zone A lavas (Fig. **F12**). They constitute one of the highest Na8 populations from major mid-ocean spreading centers, consistent with deep axial depths and low extents of melting (Klein and Langmuir, 1987). All PMM lavas have lower Na8 and higher Fe8, consistent with greater mean extents and deeper mean depths of melting. Leg 187 IMM lavas do not have the high Na_2O contents of their near-axis counterparts. Their Na8-Fe8 values overlap a high-Na8 subset of the near-axis PMM field, whereas Leg 187 PMM lavas overlap a different, lower-Na8 subfield. Other characteristics of IMM lavas that are consistent with lower extents and/or shallower depths of melting include higher SiO_2 and Al_2O_3, lower CaO, and generally lower CaO/Al_2O_3 than PMM lavas of the same age group. In all these parameters, the differences between Leg 187 IMM and PMM lavas are similar to those between the near-axis populations, but the boundary is shifted toward, or into, the on-axis PMM field (Fig. **F11**).

Major and minor element parameters that most strongly reflect source composition include TiO_2 and K_2O, in addition to Na_2O (Fig. **F11A**). Near-axis IMM lavas have lower TiO_2 at a given MgO content (Fig. **F11A**) than all other AAD region lavas. This distinction is inconsistent with lower extents of melting, suggesting a difference in source composition. In contrast to this apparent source depletion, K_2O and K/Ti values for near-axis IMM lavas are higher and more variable than expected for a simple decrease in extent of melting. This variability suggests a variable and complex source composition. Leg 187 lavas also fall into separate IMM and PMM fields for some but not all elements. These fields differ from each other in the same sense as the near-axis IMM and PMM fields but with field boundaries displaced toward and partially or completely overlapping the near-axis PMM fields (Figs. **F8, F11**). In terms of incompatible trace element contents, near-axis IMM lavas have high Ba/La, Ba/Zr, and La/Sm ratios relative to all other AAD region lavas (Fig. **F11B**). Leg 187 IMM lavas have generally lower values of these ratios, but both IMM groups define distinct fields that have little or no overlap with PMM lavas. These differences are consistent in direction with lower extents of melting for IMM lavas, but their magnitude is too great to be solely attributable to extent of melting.

Overall, the contrasts between near-axis IMM lavas, Leg 187 IMM lavas, and all PMM lavas seem to be primarily related to lower extents of

F11. Element variations illustrating contrasts between PMM and IMM, p. 36.

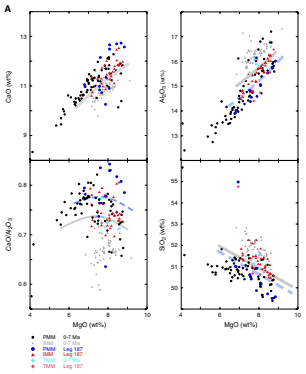

F12. Na8-Fe8 diagram showing trend of global array, p. 38

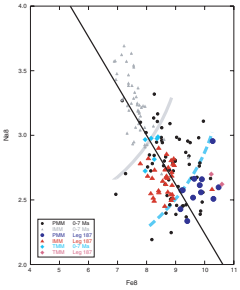

melting in the Indian domain that have diminished significantly through time. In parallel with this apparent decrease, there appears to have been an overall increase in incompatible element contents, reflecting greater contributions to individual lavas from an enriched source component. Whether this source component has become more abundant in recent time or whether it is simply contributing a greater fraction of the diminishing overall magma production is not yet clear.

DYNAMICS AND ORIGIN OF THE AAD

Evolution of the Melting Regime

The elemental systematics described above confirm that IMM lavas have consistently been derived by smaller degrees of melting than their PMM counterparts throughout the last ~30 m.y. More surprisingly, they indicate a marked decrease in overall degree of melting for both groups since ~14 Ma. Because there are no samples from 7- to 14-Ma seafloor, the timing and profile (whether it was gradual or incremental) of this decrease are unclear. However, the absence of discernible temporal or spatial gradients in either the 14- to 28-Ma Leg 187 data set or the 0- to 7-Ma near-axis data set suggests that the decrease may have been relatively abrupt and related to either or both of two significant tectonic events documented in tectonic reconstructions by Marks et al. (1999). Between ~14 and 12 Ma, both the deep central axis of the depth anomaly and (1–2 m.y. later) the IMM/PMM mantle boundary were relocated from Zone A to Zone B as a consequence of the northeastward migration of the 127°E Fracture Zone (e.g., Marks et al., 1999). At about the same time, the boundary between Segments B3 and B4 first developed as a permanent offset of the SEIR. This boundary is not a typical transform. Its position along axis is unstable (Marks et al., 1999), and it currently separates zones in which amagmatic, listric spreading has maintained opposite polarities for at least several million years (Okino et al., submitted [N2]).

We speculate that the new spatial coincidence of the AAD with cool mantle beneath the AADA led to decreased magma production and to the onset of pronounced and persistent amagmatic spreading including the separation of Segments B3 and B4. A second possible cause of the decrease in magma production can be related to an apparent broadening of the depth anomaly along axis. If one assumes that the depth anomaly became locked into the lithosphere close to the spreading axis (cf. Marks et al., 1999), then at ~8 Ma the depth anomaly began to expand to the west along the SEIR, almost doubling its along-axis extent by the present day (Marks et al., 1999; Gurnis et al., 1998). Expansion of the depth anomaly, reflecting cooling of the underlying mantle, would also account for decreased melt production. This hypothesis is consistent with dynamic models that indicate the relatively recent entrainment of residual slab material into the upwelling mantle beneath the AAD (Gurnis et al., 1998). If, however, the key assumption is incorrect and the depth anomaly did not lock in until the lithosphere was several million years old, then this hypothesis is difficult to sustain, as the apparent expansion of the depth anomaly is at least partly a dynamic phenomenon related to the spreading process.

Constraints on the Origin of the AAD and the AADA

Geophysical Evidence for Entrainment of a Residual Arc Source

Gurnis et al. (1998) and Gurnis and Müller (2003) proposed a detailed model for the origin of the AAD and the AADA. Based on dynamic plate motion reconstructions in a fixed mantle reference frame, they showed that the cold north-south elongate "source" of the depth anomaly coincides with the location of a long-lived, pre-100-Ma western Pacific subduction zone. The low mantle temperature beneath the AADA is inferred to derive from refractory subducted material that accumulated at the 660-km mantle discontinuity beneath this subduction zone. Furthermore, their mantle flow models incorporating this hypothesis indicate relatively recent (<20 Ma) entrainment of some of this refractory material along with overlying mantle wedge material into the upwelling upper mantle beneath the AAD. Cooling associated with this entrainment could potentially explain aspects of the evolution of the AAD, including the onset of its crenellated geometry.

One specific prediction of the entrainment model is a relatively recent reduction in mantle temperature beneath the AAD. The principal evidence that points to recent cooling of the mantle is discussed in the preceding sections. It includes the recent (<8 Ma) expansion of the depth anomaly and possibly the relatively recent (specific age unknown, but <14 Ma) increase in Na_2O contents of IMM lavas. However, the onset of both effects is rather more recent than the ~20-Ma initiation of the present crenellated plate boundary geometry that defines the onset of the cooling effect proposed by Gurnis and Müller (2003).

Despite these qualitatively consistent effects, the hypothetical entrainment of deep refractory mantle is questionable. Despite the compositional and thermal contrasts inherent in the tectonics of the AAD region, the Gurnis et al. (1998) and Gurnis and Müller (2003) models employ a uniform viscosity through the entire upper mantle. This simplified assumption has profound effects on model mantle flow patterns, and the results differ significantly from those of mantle flow models that explicitly incorporate variable mantle viscosity (West, 1997; West et al., 1997; Lin et al., 2002). In the three-dimensional models of West et al., incorporation of a cold, viscous region into the lower part of the upper mantle leads to preferential lateral inflow in the shallow mantle beneath the SEIR for a wide range of model parameters. This lateral flow replaces material removed by spreading while the cold region remains immobile due to its high viscosity. Lin et al. (2002) used dynamic variable-viscosity models to explicitly explore conditions under which cold mantle could upwell beneath the AAD. They concluded that for realistic viscosity structures, upwelling of cooler material is feasible only in relatively close proximity to thick continental lithosphere and is not sustainable in the long term. In this scenario, upwelling of cold residual arc material may have been initiated at ~45 Ma, when the present phase of relatively rapid spreading began, but entrainment of this material would have ceased by ~20 Ma. Thus, the degree of entrainment would diminish through time in the opposite sense to that inferred by Gurnis and Müller.

Geochemical Evidence for Entrainment

In principle, the entrainment model predicts that there should be an increasingly recognizable geochemical signal derived from the entrained subduction complex in progressively younger IMM lavas, but the nature of such a signal is difficult to predict. It could be dominated either by subducted material or by material from the original mantle wedge. If the latter, it could be characteristic of arc magmas derived from a "subduction-enriched" mantle wedge or it could have the "inverse" characteristics expected for a residual mantle wedge that was highly depleted as a consequence of arc melt production.

All IMM lavas have high Ba contents relative to PMM, and this distinction is more pronounced for near-axis lavas relative to those from Leg 187 sites (Fig. F8) (Christie, Pederson, Miller, et al., 2001). Taken at face value, these contrasts are in a sense predicted for a subduction-enriched signal, but Ba contents of IMM lavas are generally within the normal MORB range and the signature Nb depletion that typically accompanies Ba enrichment in volcanic arc settings is completely absent from the AAD region (C.J. Russo et al., pers. comm., 2004). PMM lavas are Ba depleted relative to their IMM counterparts and to normal MORB. Ba depletion could be consistent with inverse models invoking a depleted mantle wedge, but if that were the case, the strongest Ba depletion should be in IMM lavas and not, as observed, in PMM lavas.

Kempton et al. (2002) considered the potential geochemical consequences of subduction modification of a MORB mantle and proposed a multistage process involving initial depletion of a MORB mantle wedge, followed by subduction enrichment and radiogenic ingrowth. This model allows for a distinctive arc signature to be retained only in the relatively immobile Hf-Nd isotopic ratios of the wedge material with all other incompatible elements having been entirely removed in fluids. This allows for the relatively high εHf values of Zone A west lavas (13–15) to have been developed by radiogenic ingrowth of subduction-modified MORB mantle over periods of 500–1500 m.y. for reasonable parental Lu/Hf ratios. Based on this model, Kempton et al. (2002) argued that high-εHf Leg 187 IMM lavas from Zone A west are derived from such a subduction-modified mantle wedge and that this high εHf source has since expanded geographically, consistent with the entrainment model, to almost exclusively feed Zones B and C at present.

Unfortunately, two significant problems cast doubt on this interpretation. First, the entrainment model as proposed should impart a distinctive geochemical signature to the IMM/PMM boundary region that is not associated with the IMM province overall. This is not apparent from available data. Second, the model appears to require radiogenic ingrowth times that are significantly longer than allowed by the geodynamic constraints. These issues are discussed in the remainder of this section.

Confirmation of the entrainment model depends on a geochemical signature that is uniquely identified with the IMM/PMM boundary region and that expands along axis as entrainment proceeds. In terms solely of εHf, newly available data (Fig. F13) (Hanan et al., 2000a, 2000b, submitted [N1]) appear to confirm that relatively high εHf lavas (>13) occur throughout Segments B5 to B3, but their distribution is unconstrained to the west due to lack of data. In Segments B3 and B4, the diversity of εHf values reflects an overall extreme isotopic diversity (Pyle et al., 1992) that is not present in Zone A west. This diversity reflects, at least in part, a very low magma supply associated with the pre-

F13. εHf relative to the IMM/PMM boundary, p. 39.

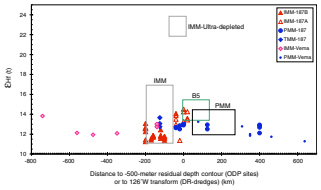

dominantly amagmatic spreading regime in these segments (Pyle et al., 1992; Christie et al., 1998) and is inconsistent with the Kempton et al. model in which the subduction-related signal is preserved solely in the Hf-Nd isotopic systematics.

On a broader scale, with the exception of several ultra-depleted lavas (εHf > 20), all AAD and Zone A lavas lie within the lower third of the known range for Indian Ocean MORB (Pearce et al., 1999; Kempton et al., 2002). This suggests that the locally high εHf values of the Leg 187 Zone A west sites and of Zone B axial lavas are a subset of a widespread IMM population and not a unique feature of the IMM/PMM boundary region. Hanan et al. (2000a, 2000b, submitted [N1]) have interpreted the higher εHf values among the broad array of IMM isotopic compositions in terms of mixing toward a widespread Archean subcontinental contaminant. In this respect it is noteworthy that a projection of the isotopic boundary trace would intersect the continent close to the eastern boundary of the Australian craton.

Finally, the time required by this model (>500 Ma) for radiogenic ingrowth appears to be too long to be consistent with the geodynamic constraints. According to the Gurnis et al. (1998) and Gurnis and Müller (2002) tectonic model, the original western Pacific subduction zone was overridden by the Australian plate and subduction ceased at ~100 Ma. Assuming a relatively old mean age for downgoing lithosphere of ~100 Ma and assuming that subduction operated at this location for ~100 m.y., the mean age of accumulated subducted material is unlikely to be significantly older than ~250 Ma, providing insufficient time for radiogenic ingrowth in a modified slab or mantle wedge with reasonable initial Lu/Hf.

The need for long radiogenic ingrowth times is particularly acute for several ultra-depleted, very high εHf IMM lavas from the AAD. Data of Salters (1996) and Hanan et al. (2000a, 2000b, submitted [N1]) include εHf values >20 at four sites in Segment B4 that are among the highest εHf values reported from the Indian Ocean. They are confined to regions of chaotic seafloor terrain formed by predominantly amagmatic, listric extensional faulting (Christie et al., 1998) where they are interspersed with low-εHf lavas (Fig. F13). They presumably represent a minor mantle component that is clearly manifested in lava compositions only when melting is limited to small intermittent batches. Although the known ultra-depleted lavas are spatially associated with the IMM/PMM boundary, Hanan et al. (2000a, 2000b, submitted [N1]) argued that an ultra-depleted end-member component is widespread as in normal Indian Ocean mantle. Regardless of its geographic extent, this component is unlikely to be derived from a relatively young upper Paleozoic–Mesozoic arc source, as there is insufficient time available for radiogenic ingrowth. Older potential source materials of both arc and cratonic origin are readily available farther to the west within or beneath the Australian continental crust.

SUMMARY AND CONCLUSIONS

We have achieved the principal objective of ODP Leg 187: using isotopic compositions of Leg 187 basalt glasses to map the Indian/Pacific MORB mantle domain boundary location throughout the last 25–30 m.y. The IMM/PMM boundary is an intrinsic feature of the AADA, and this geometry precludes a long-standing alternative hypothesis involving long-term, sustained rapid migration of PMM from the east. Leg 187

isotope systematics enable us to locate the off-axis trace of the isotopic boundary with remarkable precision, within ±50 km. For the last ~25 m.y., the boundary has been located ~100 km east of the midline of the residual depth anomaly, between the –400- and –500-m depth anomaly contours (Fig. F2). A pronounced westward deviation of the boundary trace near Sites 1158 and 1157 is interpreted as the record of a transient westward propagation event that culminated at ~20 Ma. This event is very similar in scale and duration to the well-documented recent (3–4 Ma) westward propagation of the PMM source beneath the SEIR in the easternmost AAD, displacing the preexisting IMM source. To the north of the Leg 187 work area (<42°S and >26 Ma), sample density is sparse and the boundary is poorly constrained.

A remarkable and unexpected outcome of Leg 187 is the observation that near-axis IMM lavas differ from their Leg 187 counterparts in important aspects of their trace and major element compositions and in the range and diversity of their isotopic compositions. Many of the elemental differences are in parameters that are most strongly influenced by depth and extent of melting, but differences in source composition are also apparent. Overall, IMM basalts are less evolved with a smaller range of generally higher MgO contents than their PMM counterparts. IMM lavas are also more variable in most other major and trace element contents at constant MgO, indicating their derivation from a more variable melting regime. In contrast, PMM lava compositions extend over a broader range of MgO values but are relatively invariant at a given MgO content, suggesting relatively uniform melting conditions and a dominant control by crystal fractionation processes. IMM lavas have consistently been derived by smaller degrees of melting than their PMM counterparts throughout the last ~30 m.y. Quantitatively, this difference shifted during the period of 14–7 Ma, for which there are no samples, with a significant apparent decrease in overall degree of melting for both groups. We infer that the decrease was related to the ~14- to 12-Ma relocation of the AADA and the IMM/PMM boundary from Zone A to Zone B as a consequence of the northeastward migration of the 127°E Fracture Zone that forms the eastern boundary of the AAD.

Dynamic plate motion reconstructions by Gurnis et al. (1998) and Gurnis and Müller (2003) suggest that the trace of the AADA through time, and the current location of the AAD, coincide with the location in a fixed mantle reference frame of a long-lived, pre-100-Ma western Pacific subduction zone. Low mantle temperatures beneath the AADA are inferred to derive from refractory subducted material accumulated in the lowermost upper mantle beneath this subduction zone. Mantle flow models incorporating this dynamic hypothesis suggest relatively recent (<20 Ma) entrainment of arc-derived material into the upwelling upper mantle. Although the relatively recent changes in apparent extent of melting beneath the AAD are qualitatively consistent with the entrainment aspects of this model, basalt glasses from Leg 187 and from young dredges do not display any of an array of possible geochemical signatures that could be associated with the subduction environment. We also argue that Hf-Nd isotopic systematics are consistent with a mantle source that is too old and too widespread to be derived from a Mesozoic subduction complex (this argument is controversial—see Kempton et al., 2002). Physically, the entrainment model is also suspect because it does not allow for realistic mantle viscosity gradients.

We conclude that the IMM/PMM boundary has been associated with the residual depth anomaly (AADA) through most or all of the separation of Australia from Antarctica. The origin of the distinctive isotopic

characteristics of the two provinces remains controversial and has most recently been discussed by Hanan et al. (2000a, 2000b, submitted [N1]) and Kempton et al. (2002), but it seems clear that a significant component of the IMM source must have been derived from ancient continental material as a by-product of the breakup of Gondwana. This conclusion does not preclude an arc source for much of this material, though the need for long ingrowth times to establish observed Hf-Nd isotope ratios seems to preclude a young (Mesozoic) arc source. Prior to ~12 Ma, the AAD and the AADA were geographically separate entities that have subsequently been brought into conjunction by the northeastward absolute motion of the Australian/Antarctic plate boundary. We postulate that as this conjunction came about, cooler mantle temperatures were established beneath the AAD. This led, in turn, to reduced overall extents of melting, reduced magma supply to the intermediate-spreading SEIR, and the establishment of an extensional regime dominated by listric faulting (Christie et al., 1998). Young IMM lavas from the AAD are, therefore, most likely formed by a low-degree, relatively discontinuous melting process that allows the full diversity of the complex IMM source region to be expressed in lava geochemistry. The origin of the AAD as a morphologically anomalous section of the SEIR appears to precede the maximum influence of the depth anomaly. A clear explanation for its onset may have to await a better understanding of the dynamics of this unique region.

REFERENCES

Alvarez, W., 1982. Geological evidence for the geographical pattern of mantle return flow and the driving mechanism of plate tectonics. *J. Geophys. Res.,* 87:6697–6710.

Alvarez, W., 1990. Geologic evidence for the plate driving mechanism: the continental undertow hypothesis and the Australian-Antarctic Discordance. *Tectonics,* 9:1213–1220.

Cande, S.C., LaBrecque, J.L., Larson, R.L., Pitmann, W.C., III, Golovchenko, X., and Haxby, W.F., 1989. *Magnetic Lineations of the World's Ocean Basins.* AAPG Map Ser., 13.

Christie, D.M., Pedersen, R.B., Miller, D.J., et al., 2001. *Proc. ODP, Init. Repts.,* 187 [Online]. Available from World Wide Web: <http://www-odp.tamu.edu/publications/187_IR/187ir.htm>.

Christie, D.M., West, B.P., Pyle, D.G., and Hanan, B.B., 1998. Chaotic topography, mantle flow and mantle migration in the Australian-Antarctic Discordance. *Nature,* 394:637–644.

DeMets, C., Gordon, R.G., and Argus, D.F., 1988. Intralplate deformation and closure of the Australia-Antarctica-Africa plate circuit. *J. Geophys. Res.,* 93:11877–11897.

DeMets, C., Gordon, R.G., Argus, D.F., and Stein, S., 1990. Current plate motions. *Geophys. J. Internat.,* 101:425–478.

Dosso, L., Bougault, H., Beuzart, P., Calvez, J.-Y., and Joron, J.-L., 1988. The geochemical structure of the South-East Indian Ridge. *Earth Planet. Sci. Lett.,* 88:47–49.

Dupré, B., and Allègre, C.J., 1983. Pb-Sr isotope variation in Indian Ocean basalts and mixing phenomena. *Nature,* 303:142–146.

Fisk, M.R., Giovannoni, S.J., and Thorseth, I.H., 1998. Alteration of oceanic volcanic glass: textural evidence of microbial activity. *Science,* 281:978–980.

Forsyth, D.W., Ehrenbard, R.L., and Chapin, S., 1987. Anomalous upper mantle beneath the Australian-Antarctic Discordance. *Earth Planet. Sci. Lett.,* 84:471–478.

Furnes, H., Thorseth, I.H., Tumyr, O., Torsvik, T., and Fisk, M.R., 1996. Microbial activity in the alteration of glass from pillow lavas from Hole 896A. *In* Alt, J.C., Kinoshita, H., Stokking, L.B., and Michael, P.J. (Eds.), *Proc. ODP, Sci. Results,* 148: College Station, TX (Ocean Drilling Program), 191–206.

Gurnis, M., and Müller, R.D., 2003. Origin of the Australian-Antarctic Discordance from an ancient slab and mantle wedge. *In* Hills, R.R., and Müller, R.D. (Eds.), *Evolution and Dynamics of the Australian Plate.* Spec. Pap.—Geol. Soc. Am., 372:417–429.

Gurnis, M., Muller, R.D., and Moresi, L., 1998. Cretaceous vertical motion of Australia and the Australian-Antarctic Discordance. *Science,* 279:1499–1504.

Hamelin, B., and Allègre, C.-J., 1985. Large-scale regional units in the depleted upper mantle revealed by an isotope study of the South-West Indian Ridge. *Nature,* 315:196–199.

Hamelin, B., Dupré, B., and Allègre, C.J., 1986. Pb-Sr-Nd isotopic data of Indian Ocean ridges: new evidence of large-scale mapping of mantle heterogeneities. *Earth Planet. Sci. Lett.,* 76:288–298.

Hanan, B.B., Blichert-Toft, J., Kingsley, R., and Schilling, J.-G., 2000a. Depleted Iceland mantle plume geochemical signature: artifact of multicomponent mixing? *Geochem., Geophys., Geosyst.,* 1:10.1029/1999GC000009.

Hanan, B.B., Blichert-Toft, J., Pyle, D.G., Christie, D., and Albarède, F., 2000b. Ultradepleted hafnium isotopes from Australian-Antarctic Discordance MORB. *J. Conf. Abstr.,* 5:478.

Hart, S.R., 1984. A large-scale isotope anomaly in the Southern Hemisphere mantle. *Nature,* 309:753–757.

Hinz, K., Hemmerich, M., Salge, U., and Eiken, O., 1990. Structures in rift-basin sediments on the conjugate margins of western Tasmania, South Tasman Rise, and Ross Sea, Antarctica. *In* Bleil, U., and Thiede, J. (Eds.), *Proceedings of the 1988 NATO*

Advanced Research Workshop on Geological History of the Polar Oceans: Arctic versus Antarctic. NATO ASI Ser., Ser. C, 308:119–130.

Kempton, P.D., Pearce, J.A., Barry, T., Fitton, J.G., Langmuir, C., and Christie, D.M., 2002. Sr-Nd-Pb-Hf isotope results from ODP Leg 187: evidence for mantle dynamics of the Australian Antarctic Discordance and origin of Indian MORB source. *Geochem., Geophys., Geosyst.,* 3:10.1029/2002GC000320.

Klein, E.M., and Langmuir, C.H., 1987. Global correlations of ocean ridge basalt chemistry with axial depth and crustal thickness. *J. Geophys. Res.,* 92:8089–8115.

Klein, E.M., Langmuir, C.H., Zindler, A., Staudigel, H., and Hamelin, B., 1988. Isotope evidence of a mantle convection boundary at the Australian-Antarctic Discordance. *Nature,* 333:623–629.

Lanyon, R., Crawford, A.J., and Eggins, S., 1995. Westward migration of Pacific Ocean upper mantle into the Southern Ocean region between Australia and Antarctica. *Geology,* 23:511–514.

Lin, S.-C., Liu, L.-Y., and Kuo, B.-Y., 2002. Dynamic interaction of cold anomalies with the mid-ocean ridge flow field and its implications for the Australian-Antarctic Discordance. *Earth Planet. Sci. Lett.,* 203:925–935.

Mahoney, J., le Roex, A.P., Peng, Z., Fisher, R.L., and Natland, J.H., 1992. Southwestern limits of Indian Ocean ridge mantle and the origin of low $^{206}Pb/^{204}Pb$ mid-ocean ridge basalt: isotope systematics of the central Southwest Indian Ridge (17°–50°E). *J. Geophys. Res., [Solid Earth Planets],* 97:19771–19790.

Mahoney, J.J., Natland, J.H., White, W.M., Poreda, R., Bloomer, S.H., Fisher, R.L., and Baxter, A.N., 1989. Isotopic and geochemical provinces of the western Indian Ocean spreading centers. *J. Geophys. Res.,* 94:4033–4052.

Marks, K.M., Stock, J.M., and Quinn, K.J., 1999. Evolution of the Australian-Antarctic Discordance since Miocene time. *J. Geophys. Res.,* 104:4967–4981.

Marks, K.M., Vogt, P.R., and Hall, S.A., 1990. Residual depth anomalies and the origin of the Australian-Antarctic Discordance zone. *J. Geophys. Res.,* 95:17325–17337.

Mutter, J.C., Hegarty, K.A., Cande, S.C., and Weissel, J.K., 1985. Breakup between Australia and Antarctica: a brief review in the light of new data. *Tectonophysics,* 114:255–279.

Palmer, J., Sempéré, J.-C., Christie, D.M., and Phipps-Morgan, J., 1993. Morphology and tectonics of the Australian-Antarctic Discordance between 123°E and 128°E. *Mar. Geophys. Res.,* 15:121–152.

Pearce, J.A., Kempton, P.D., Nowell, G.M., and Noble, S.R., 1999. Hf-Nd element and isotope perspective on the nature and provenance of mantle and subduction components in western Pacific arc-basin systems. *J. Petrol.,* 80:1579–1611.

Price, R.C., Kennedy, A.K., Riggs-Sneeringer, M., and Frey, F.A., 1986. Geochemistry of basalts from the Indian Ocean triple junction: implications for the generation and evolution of Indian Ocean ridge basalts. *Earth Planet. Sci. Lett.,* 78:379–396.

Pyle, D.G., 1994. Geochemistry of mid-ocean-ridge basalt within and surrounding the Australian-Antarctic Discordance. [Ph.D. dissert.]. Oregon State Univ., Corvallis.

Pyle, D.G., Christie, D.M., Hanan, B.B., Pedersen, R.-B., and Shipboard Science Party, 2000. Regional isotopic constraints on eastern Indian and western Pacific MORB mantle components. *Eos, Trans. Am. Geophys. Union,* 81:F1285.

Pyle, D.G., Christie, D.M., and Mahoney, J.J., 1992. Resolving an isotopic boundary within the Australian-Antarctic Discordance. *Earth Planet. Sci. Lett.,* 112:161–178.

Pyle, D.G., Christie, D.M., Mahoney, J.J., and Duncan, R.A., 1995. Geochemistry and geochronology of ancient southeast Indian and southwest Pacific seafloor. *J. Geophys. Res.,* 100:22261–22282.

Ritzwoller, M.H., Shapiro, N.M., and Leahy, G.M., 2003. The Australian-Antarctic mantle anomaly as the principal cause of the Australian-Antarctic Discordance. *J. Geophys. Res.,* 108:10.1029/2003JB002522.

Salters, V.J.M., 1996. The generation of mid-ocean ridge basalts from the Hf and Nd isotope perspective. *Earth Planet. Sci. Lett.,* 141:109–123.

Sempéré, J.-C., Palmer, J., Christie, D.M., Phipps-Morgan, J., and Shor, A.N., 1991. The Australian-Antarctic Discordance. *Geology,* 19:429–432.

Sempéré, J.-C., West, B.P., and Géli, L., 1996. The Southeast Indian Ridge between 127° and 134°40′E: contrasts in segmentation characteristics and implication for crustal accretion. *In* MacLeod, C.J., Tyler, P.A., and Walker, C.L. (Eds.), *Tectonic, Magmatic, Hydrothermal and Biological Segmentation of Mid-Ocean Ridges*. Geol. Soc. Spec. Publ., 118:1–15.

Shipboard Scientific Party, 2001. Site 1160. *In* Christie, D.M., Pedersen, R.B., Miller, D.J., et al., *Proc. ODP, Init. Repts.,* 187, 1–42 [CD-ROM]. Available from: Ocean Drilling Program, Texas A&M University, College Station TX 77845-9547, USA.

Smith, W.H.F., and Sandwell, D.T., 1997. Global seafloor topography from satellite altimetry and ship depth soundings. *Science,* 277:1956–1962.

Subbarao, K.V., and Hedge, C.E., 1973. K, Rb, Sr and $^{87}Sr/^{86}Sr$ in rocks from the Mid-Indian Ocean Ridge. *Earth Planet. Sci. Lett.,* 18:223–228.

Thorseth, I.H., Furnes, H., and Tumyr, O., 1991. A textural and chemical study of Icelandic palagonite of varied composition and its bearing on the mechanism of the glass-palagonite transformation. *Geochim. Cosmochim. Acta,* 55:731–749.

Thorseth, I.H., Pedersen, R.B., and Christie, D.M., 2003. Microbial alteration of 0–30-Ma seafloor and sub-seafloor basaltic glasses from the Australian Antarctic Discordance. *Earth Planet. Sci. Lett.,* 215:237–247.

Thorseth, I.H., Pedersen, R.B., Daae, F.L., Torsvik, V., Torsvik, T., and Sundvor, E., 1999. Microbes associated with basaltic glass from the Mid-Atlantic Ridge. *Conf. Abstr., EUG 10,* Strasbourg, 4:254.

Thorseth, I.H., Torsvik, T., Furnes, H., and Muehlenbachs, K., 1995. Microbes play an important role in the alteration of oceanic crust. *Chem. Geol.,* 126:137–146.

Torsvik, T., Furnes, H., Muehlenbachs, K., Thorseth, I.H., and Tumyr, O., 1998. Evidence for microbial activity at the glass-alteration interface in oceanic basalts. *Earth Planet. Sci. Lett.,* 162:165–176.

Veevers, J.J., 1982. Australian-Antarctic depression from the mid-ocean ridge to adjacent continents. *Nature,* 295:315–317.

Vogt, P.R., Cherkis, N.Z., and Morgan, G.A., 1983. Project Investigator—1. Evolution of the Australia-Antarctic Discordance deduced from a detailed aeromagnetic study. *In* Oliver, R.L., James, P.R., and Jago, J.B. (Eds.), *Antarctic Earth Science.* Antarct. Earth Sci., [Pap.—Int. Symp.], 4th, 608–613.

West, B.P., 1997. Mantle flow and crustal accretion in and near the Australian-Antarctic Discordance [Ph.D. thesis]. Univ. of Washington, Seattle.

West, B.P., Sempéré, J.-C., Pyle, D.G., Phipps-Morgan, J., and Christie, D.M., 1994. Evidence for variable upper mantle temperature and crustal thickness in and near the Australian-Antarctic Discordance. *Earth Planet. Sci. Lett.,* 128:135–153.

West, B.P., Wilcock, W.S.D., and Sempéré, J.-C., 1997. Three-dimensional structure of asthenospheric flow beneath the Southeast Indian Ridge. *J. Geophys. Res.,* 102:7783–7802.

Figure F1. Regional map of the Southeast Indian Ocean after Pyle et al. (1995) showing magnetic lineations (Cande et al., 1989) and DSDP sites that sampled basement (numbered solid circles). Dark line defining V-shape east of the Australian Antarctic Discordance (AAD) is the hypothetical trace of a rapidly migrating (40 mm/yr) isotopic boundary. (This hypothesis is disproved by the results of Leg 187.) Broader gray V-shape of the approximate midline (axis) of the regional depth anomaly traces a slower (15 mm/ yr) westward relative migration (Marks et al., 1990). Bull's-eye symbols are dredge sites of Lanyon et al. (1995). Boxes outline the area of operations of Leg 187 and the approximate area of Figure F2, p. 27.

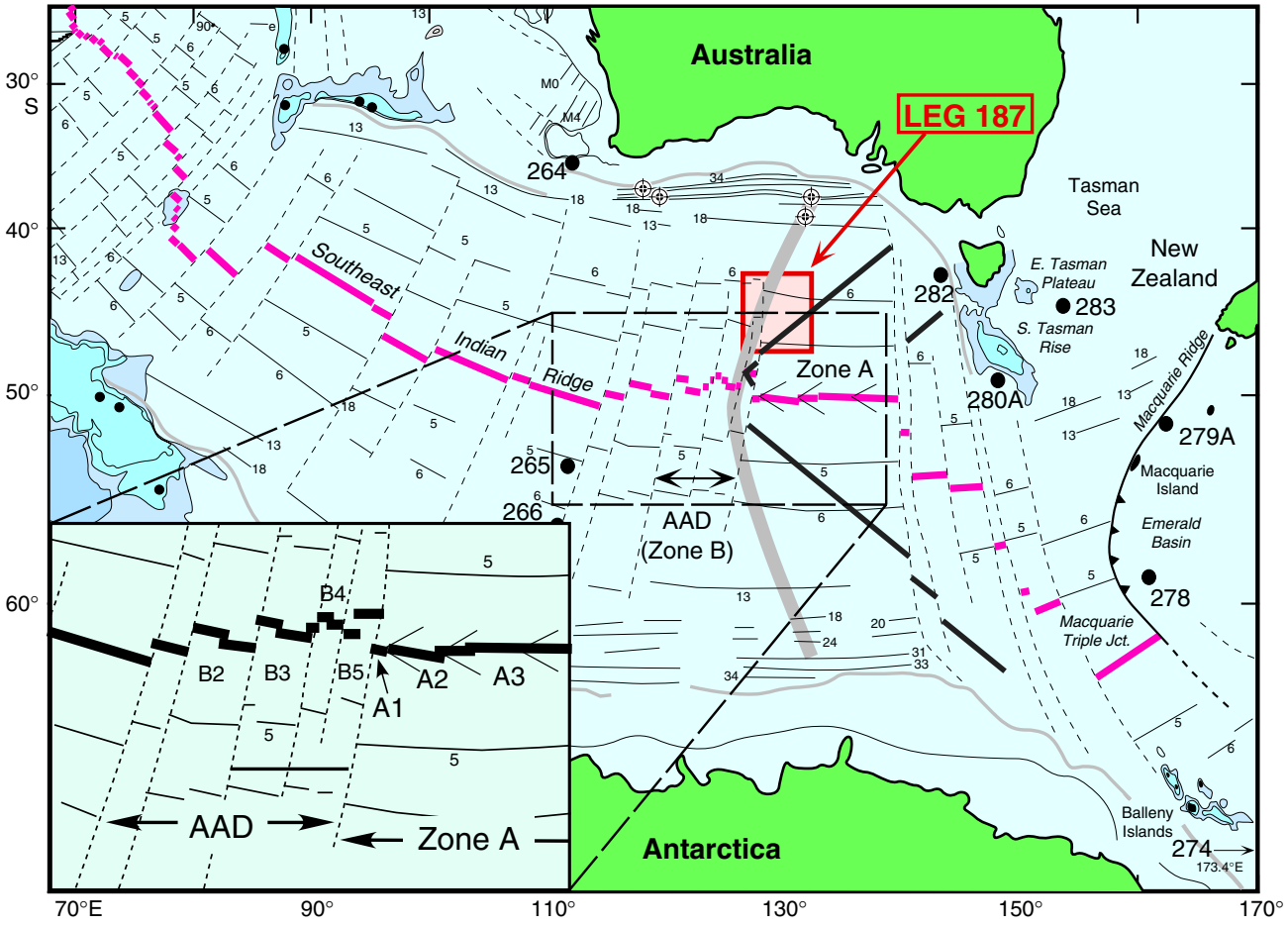

Figure F2. Satellite gravity map using data of Smith and Sandwell (1977). Contours outline residual depth anomaly (values in meters) of Marks et al. (1990). Larger circles are locations of Leg 187 sites coded as Indian Ocean MORB mantle (IMM), Pacific Ocean MORB mantle (PMM), or transitional MORB mantle (TMM) based on their isotopic compositions. "Mixed I/P" symbol indicates sites that recovered both PMM and IMM samples. Smaller circles are MW88 and BO05 dredge sites. Circles are coded for mantle domain type as determined by Pb isotopic data of D. Pyle et al. (pers. comm., 2004). Long arrows point to oblique lineations associated with rift propagation. Small arrows near 50°S indicate off-axis dredge sites referred to in text (see **"Background: Mantle Flow Hypotheses"** p. 4, in "The Indian/Pacific Mantle Isotopic Boundary." Heavy white line is the trace of the Indian/Pacific MORB mantle boundary inferred from the isotopic compositions of Leg 187 and near-axis dredged samples. FZ = fracture zone.

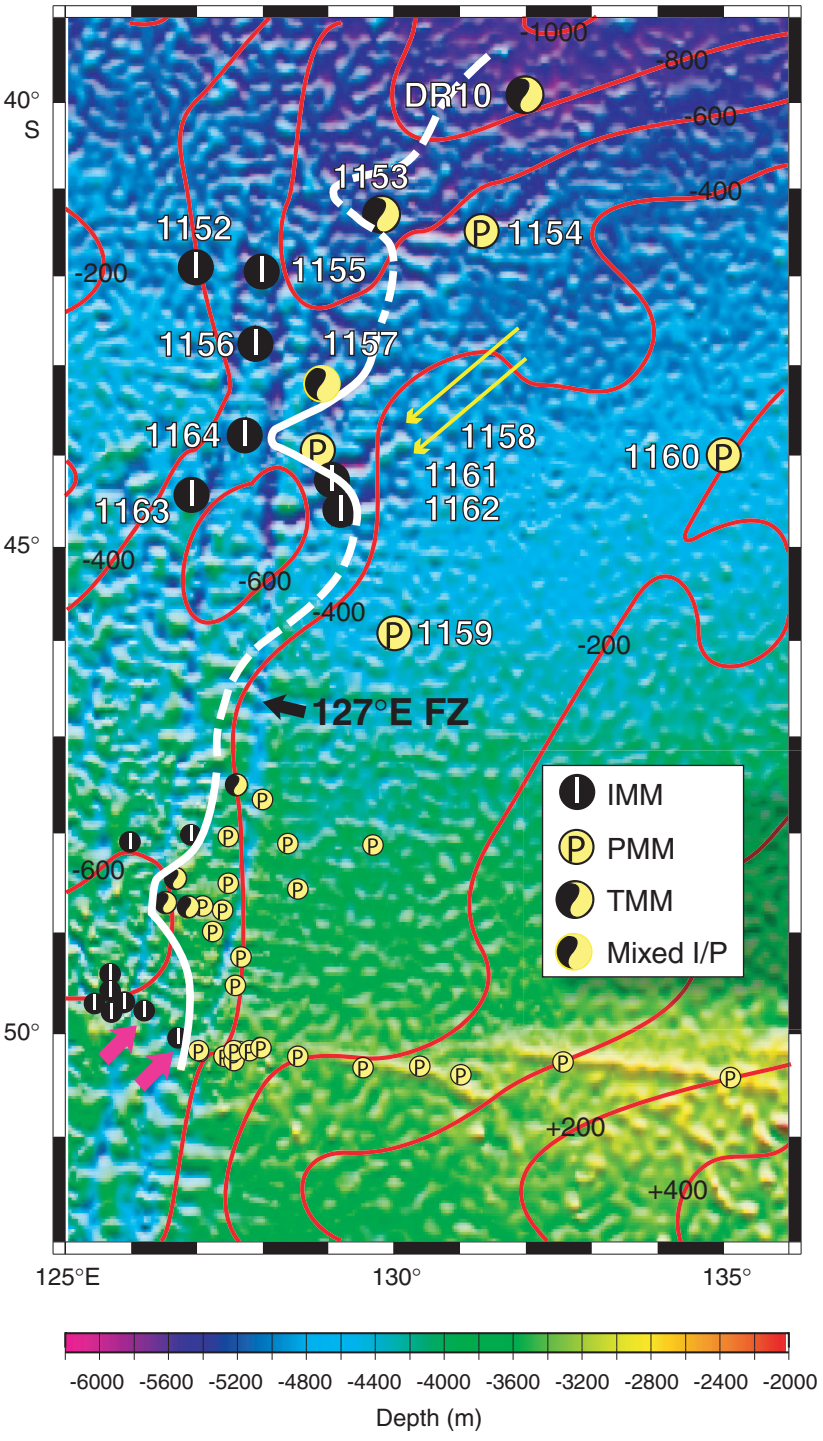

Figure F3. A. Alteration halo around a zeolite vein in fresh volcanic glass. **B.** Mn oxide–encrusted, subspherical microbial cell forms in a zeolite vein. Both images after Thorseth et al, in press.

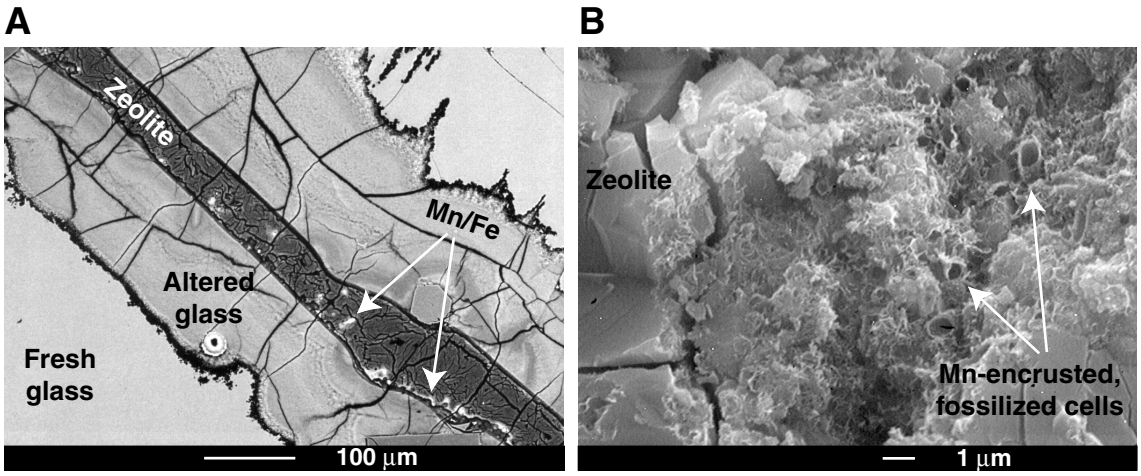

Figure F4. "Isocon plots" showing systematic interelement alteration relationships in two altered Leg 187 samples. From **Miller and Kelley** (this volume).

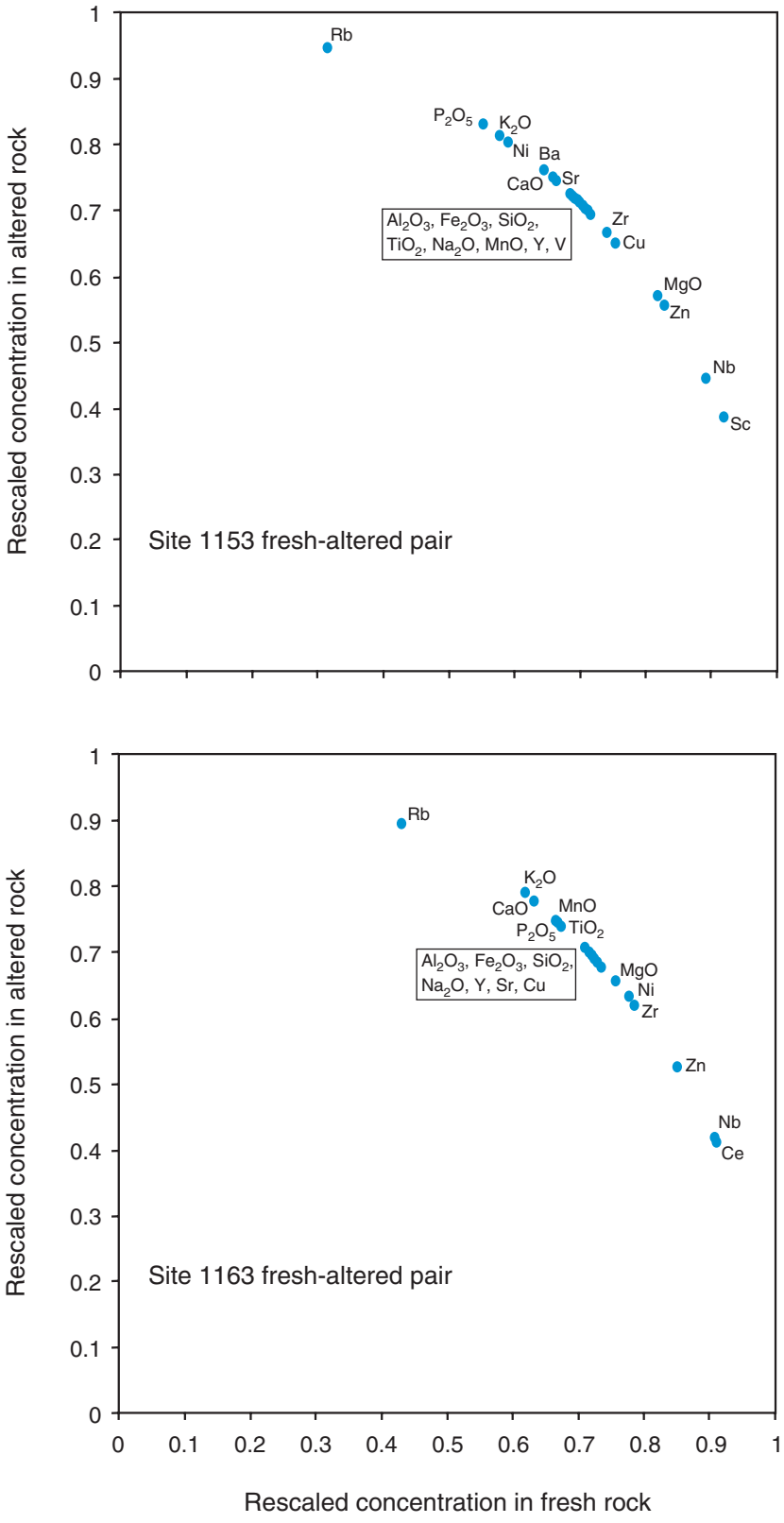

Figure F5. $^{143}Nd/^{144}Nd$ vs. $^{87}Sr/^{86}Sr$ isotopic compositions. Arrows show the water/rock proportion in representative Holes 1160B (Pacific) and 1155B (Indian). All altered samples show a shift in $^{87}Sr/^{86}Sr$ from mantle values toward seawater composition. Nd isotopic ratios are homogeneous within individual sites and remain constant during low-temperature alteration. Indian and Pacific mantle domains for fresh glass are from Pyle et al., 1992, and D. Pyle, pers. comm., 2004. Figure from S. Krolikowska-Ciaglo, F. Hauff, and K. Hoernle (pers. comm., 2003). AAD = Australian Antarctic Discordance.

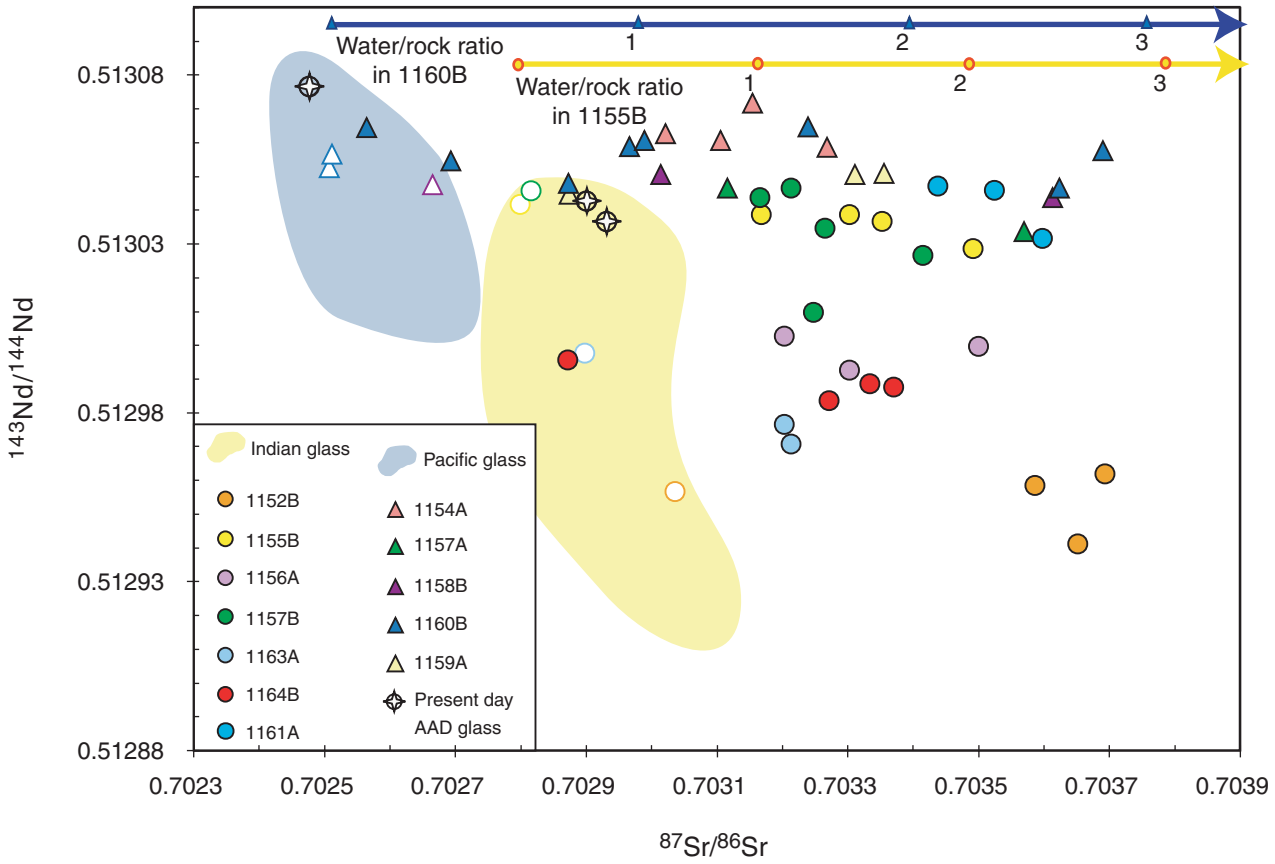

Figure F6. $^{208}Pb/^{204}Pb$ vs. $^{206}Pb/^{204}Pb$ isotopic compositions of altered samples from 11 Leg 187 sites. The Pacific mantle domain has generally more radiogenic Pb isotopic composition than Indian mantle. The analyzed sediment and vein material have the most radiogenic $^{208}Pb/^{204}Pb$ ratios. A strongly altered part of a Hole 1157A sample has similar isotopic ratios to local sediment, showing that very small amounts of sediment can drastically change the isotopic composition. $^{208}Pb/^{204}Pb$ ratios are constant at individual sites, while $^{206}Pb/^{204}Pb$ ratios are more radiogenic in the altered samples reflecting their high $^{238}U/^{204}Pb$ ratios. Figure from S. Krolikowska-Ciaglo, F. Hauff, and K. Hoernle (pers. comm., 2003). AAD = Australian Antarctic Discordance.

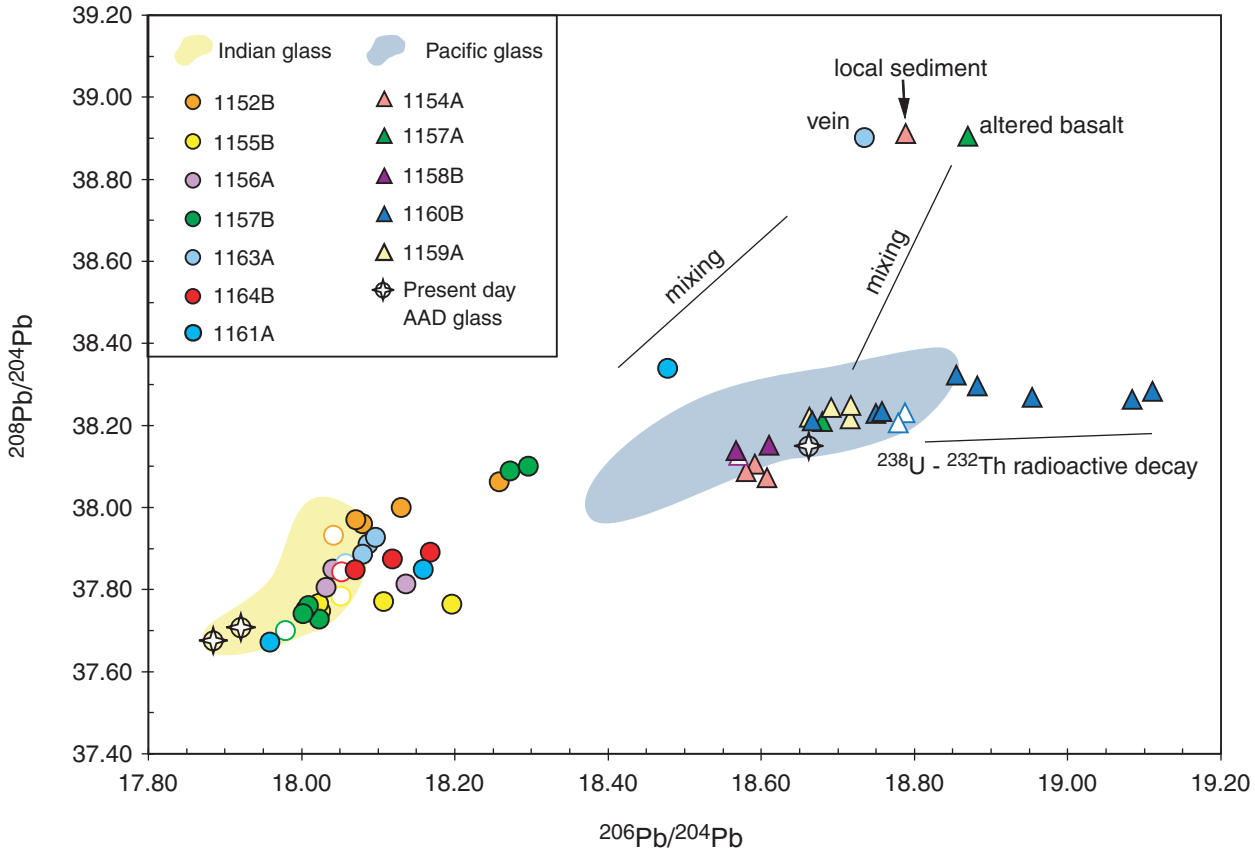

Figure F7. $^{208}Pb/^{204}Pb$ vs. $^{206}Pb/^{204}Pb$ of fresh basaltic glasses from (**A**) 0- to 7-Ma dredges described by Pyle et al. (1992, 1995) and Christie et al. (1998), outlining Indian Ocean MORB mantle (IMM), Pacific Ocean MORB mantle (PMM), and transitional MORB mantle (TMM) fields, and (**B**) from Leg 187 in relation to the near-axis data fields. Isotopic data from Pyle et al. (1992) and D. Pyle (pers. comm., 2004). Note in A that IMM and PMM are clearly discriminated by this figure. Symbols are coded according to axial segment number (A1, A2…, B5, B4…etc.). See Christie et al. (1998) or Pyle et al. (1992) for details. AAD = Australian Antarctic Discordance.

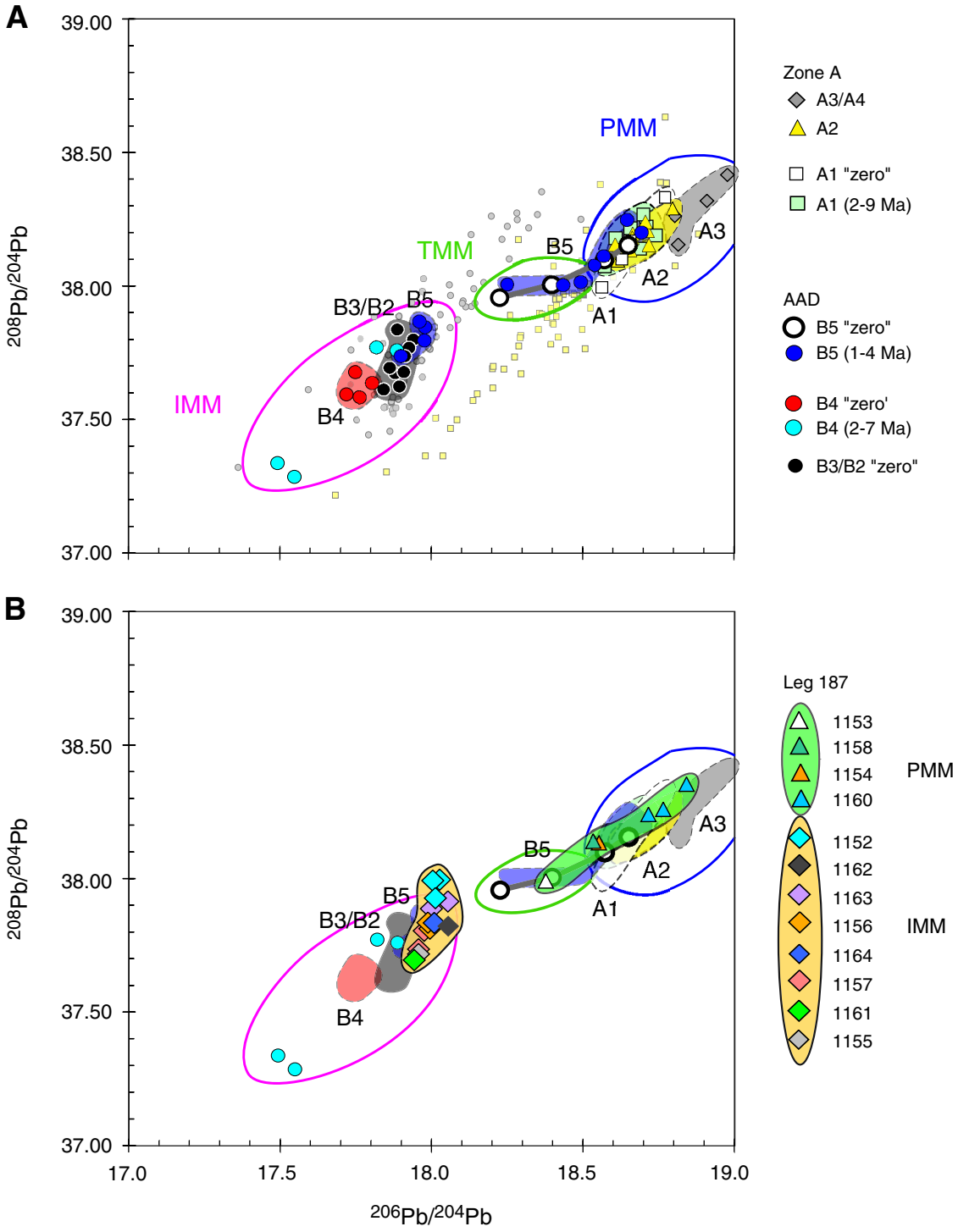

Figure F8. Ba vs. Zr/Ba plot used as a proxy to discriminate Indian from Pacific mantle domains during Leg 187. Data fields are from Christie, Pedersen, Miller, et al. (2001). Data points are Leg 187 samples coded to indicate their mantle domain type as determined from their Pb isotope compositions. Points labeled "Mixed I/P" are IMM samples from sites that recovered both PMM and IMM samples. TPMM (transitional Pacific MORB mantle) field was defined during Leg 187 using onboard data. We no longer use this term. TMM = transitional MORB mantle.

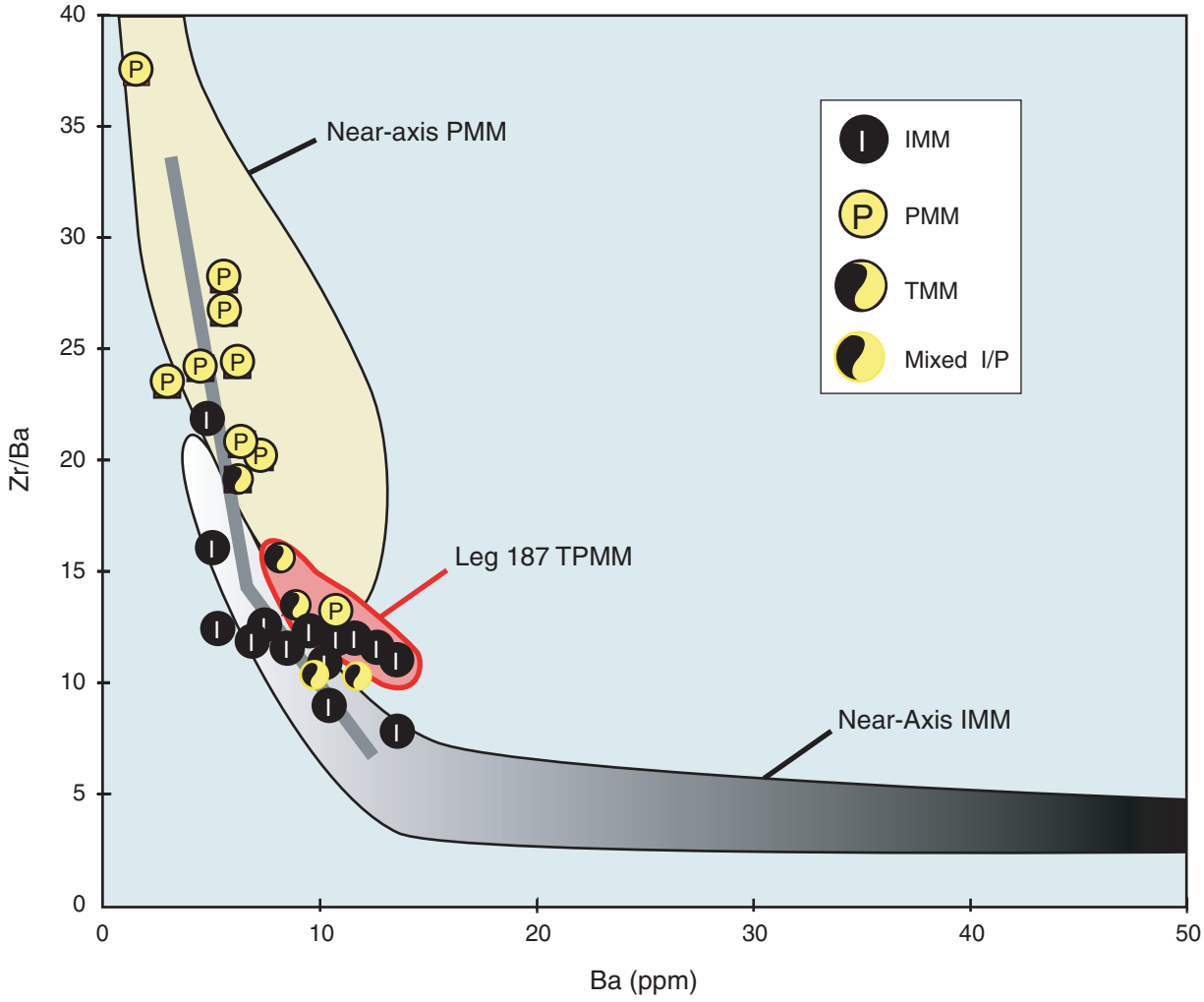

Figure F9. εNd vs. $^{206}Pb/^{204}Pb$ and $^{87}Sr/^{86}Sr$ data for Leg 187 basaltic glasses from **Pedersen et al.** (this volume). Fields outline inferred east and west mixing trends between three components that are most strongly represented at the three outlined sites (1152, 1160, and 1162).

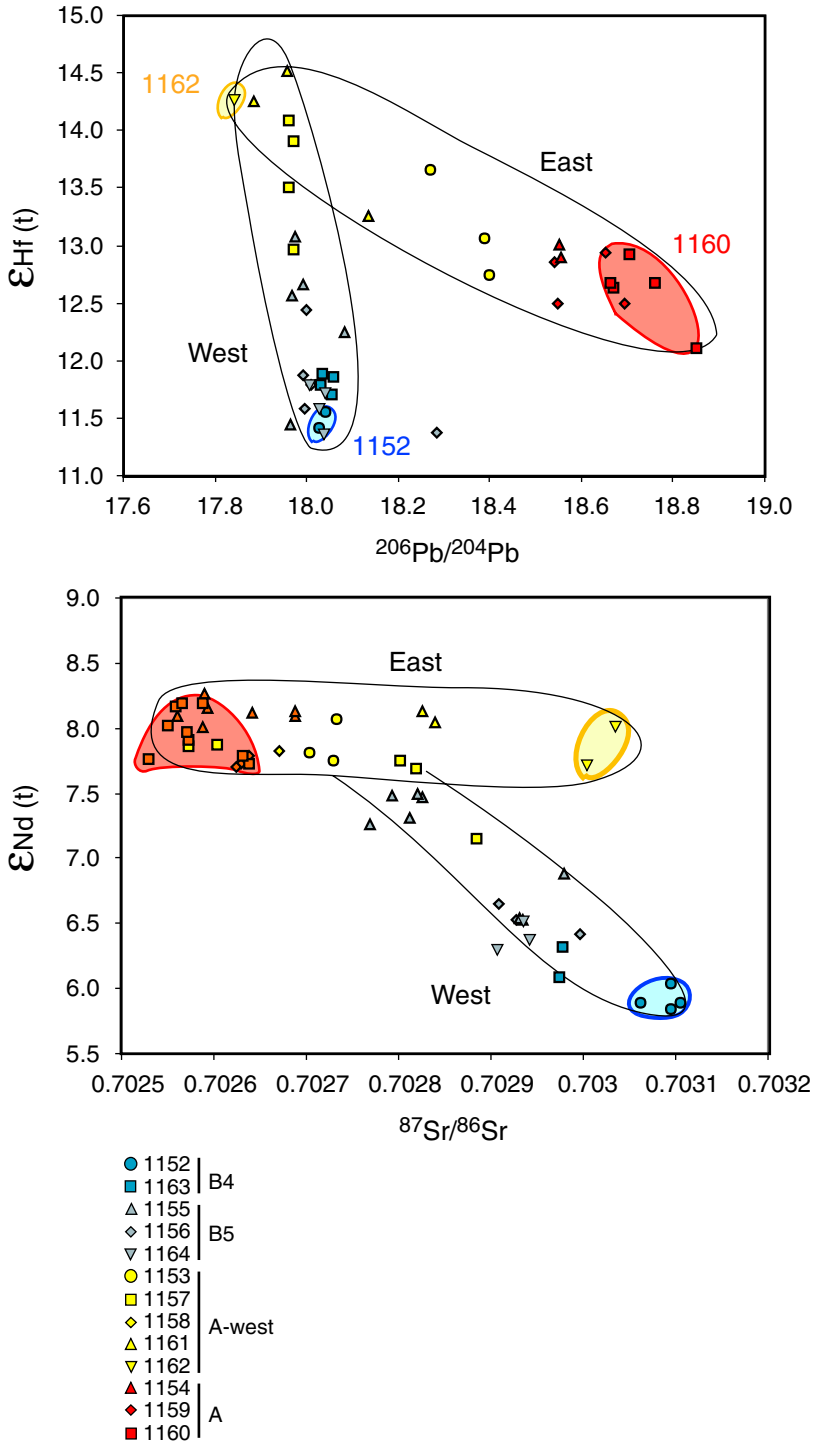

Figure F10. εHf vs. εNd diagram showing fields of all available data for the Australian Antarctic Discordance (AAD) region. Dashed line is the Indian Ocean MORB mangle (IMM)/Pacific Ocean MORB mantle (PMM) discriminant boundary of Kempton et al. (2002). Leg 187 and Vema dredge data of Kempton et al. (2002) are shown as points. Fields include all near-axis data from Hanan et al. (2000a, 2000b, submitted [N1]). TMM = transitional MORB mantle.

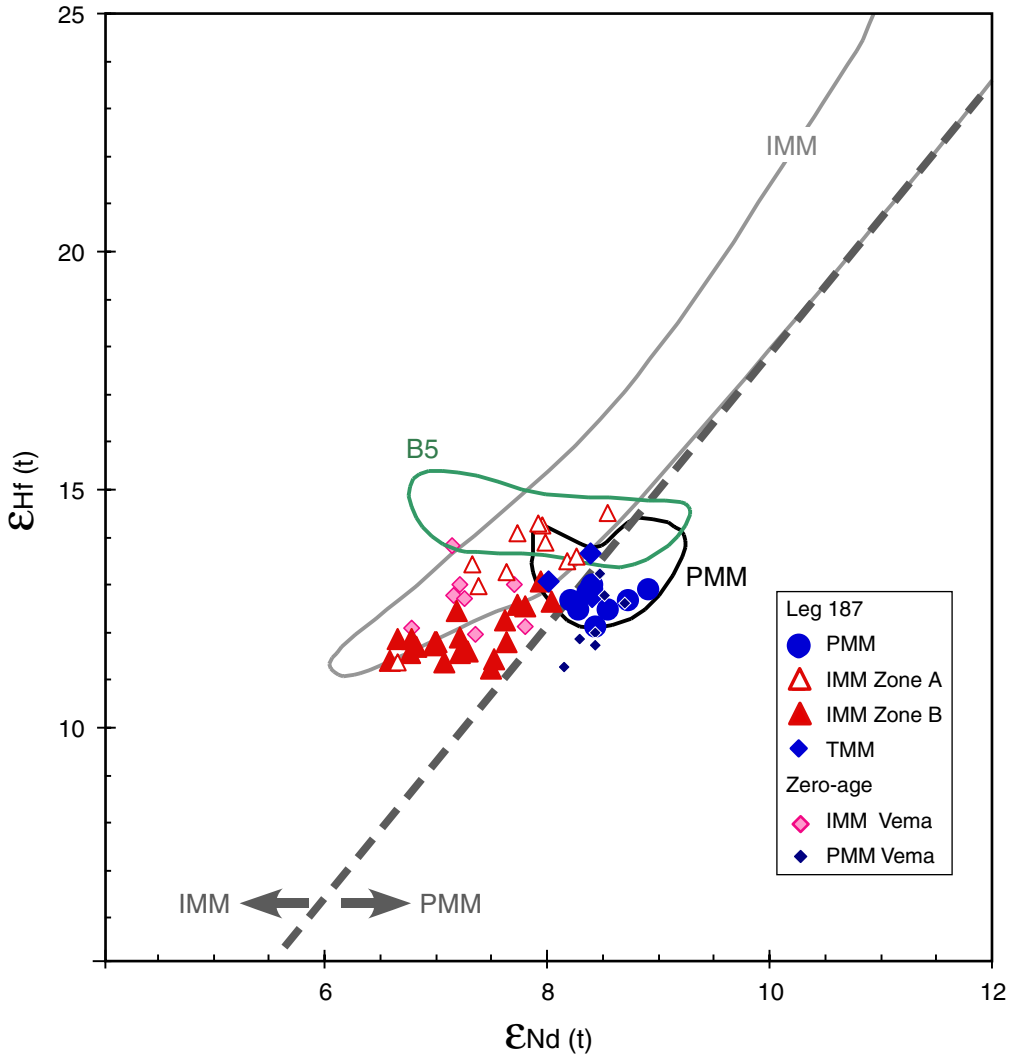

Figure F11. Major, minor, and trace element variation diagrams illustrating the contrasts between Pacific Ocean MORB mantle (PMM) and Indian Ocean MORB mantle (IMM) fields for near-axis (0–7 Ma) and Leg 187 glasses. Data from Pyle et al. (1992); D. Pyle and C.J. Russo (pers. comm., 2004). **A.** Major and minor elements. Solid line separates PMM from IMM fields for near-axis lavas only. Dashed line separates PMM from IMM fields for Leg 187 lavas, where a distinction can be made and where the field boundary differs from that for the near-axis population. TMM = transitional MORB mantle. (Continued on next page.)

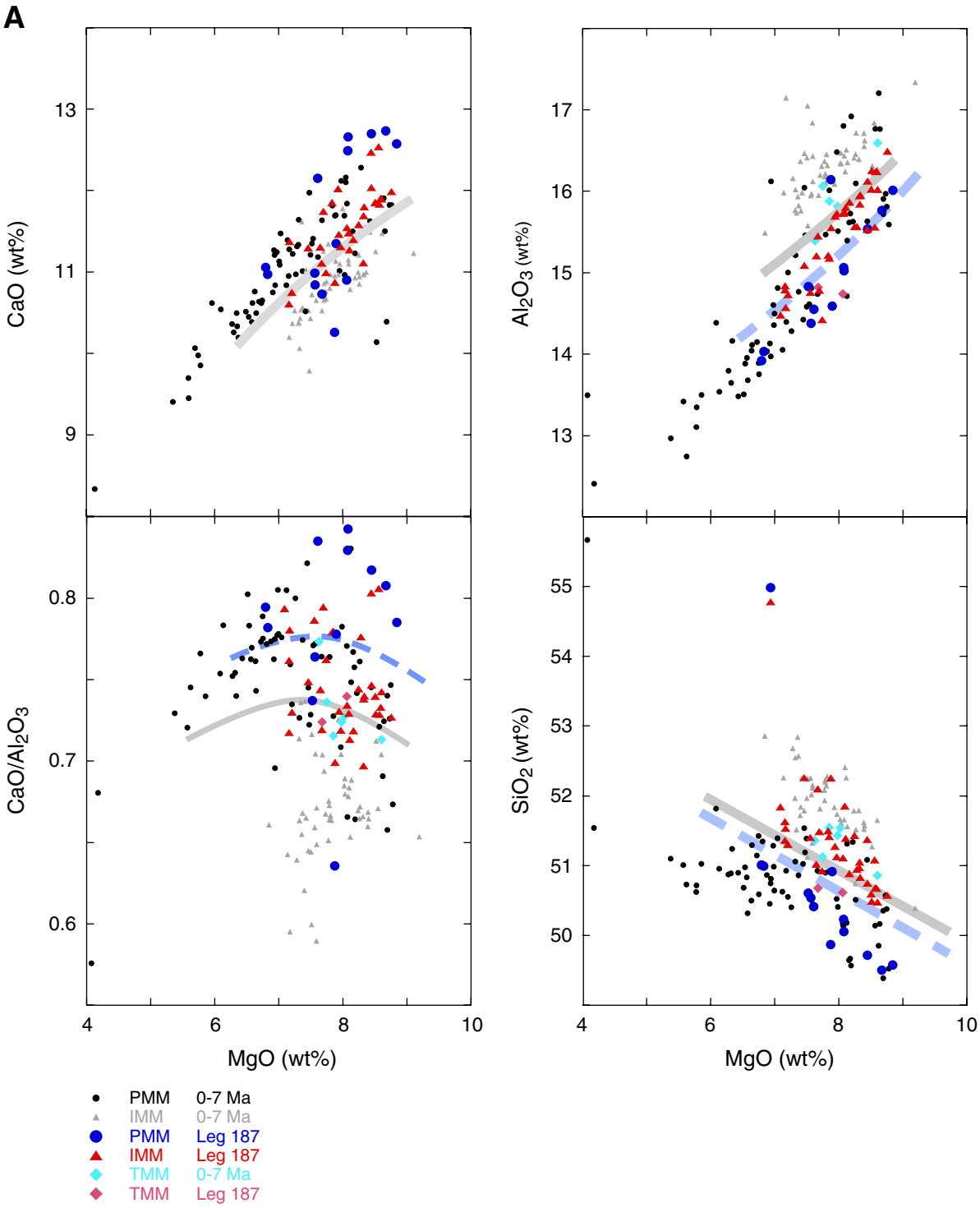

Figure F11 (continued). B. Trace elements. Dividing lines as in part A.

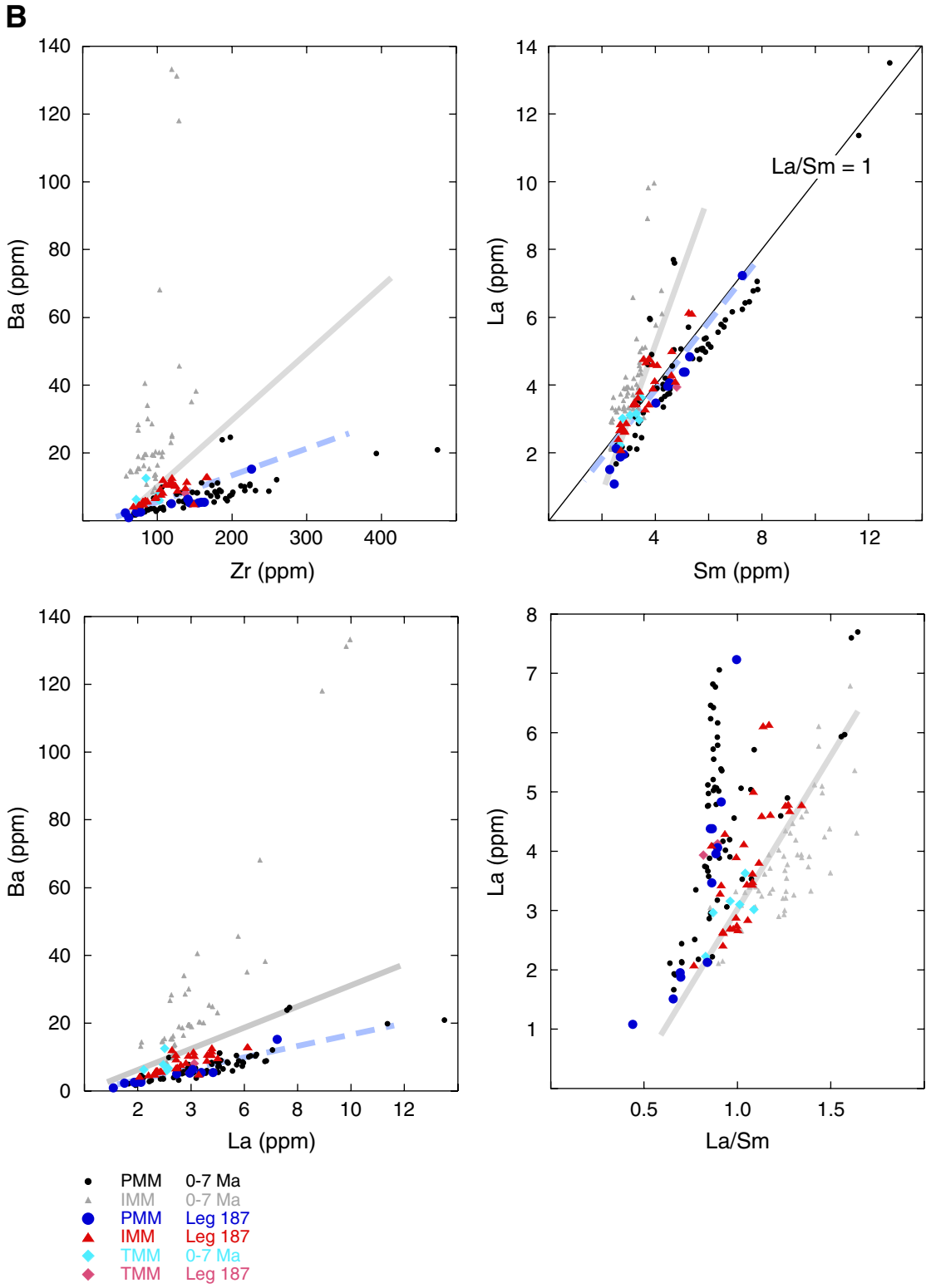

Figure F12. Na8-Fe8 diagram showing the trend of the global array after Klein and Langmuir (1987). Solid and dashed lines separate Indian Ocean MORB mantle (IMM) from Pacific Ocean MORB mantle (PMM) fields for near-axis (0–7 Ma) and Leg 187 lavas, respectively. TMM = transitional MORB mantle.

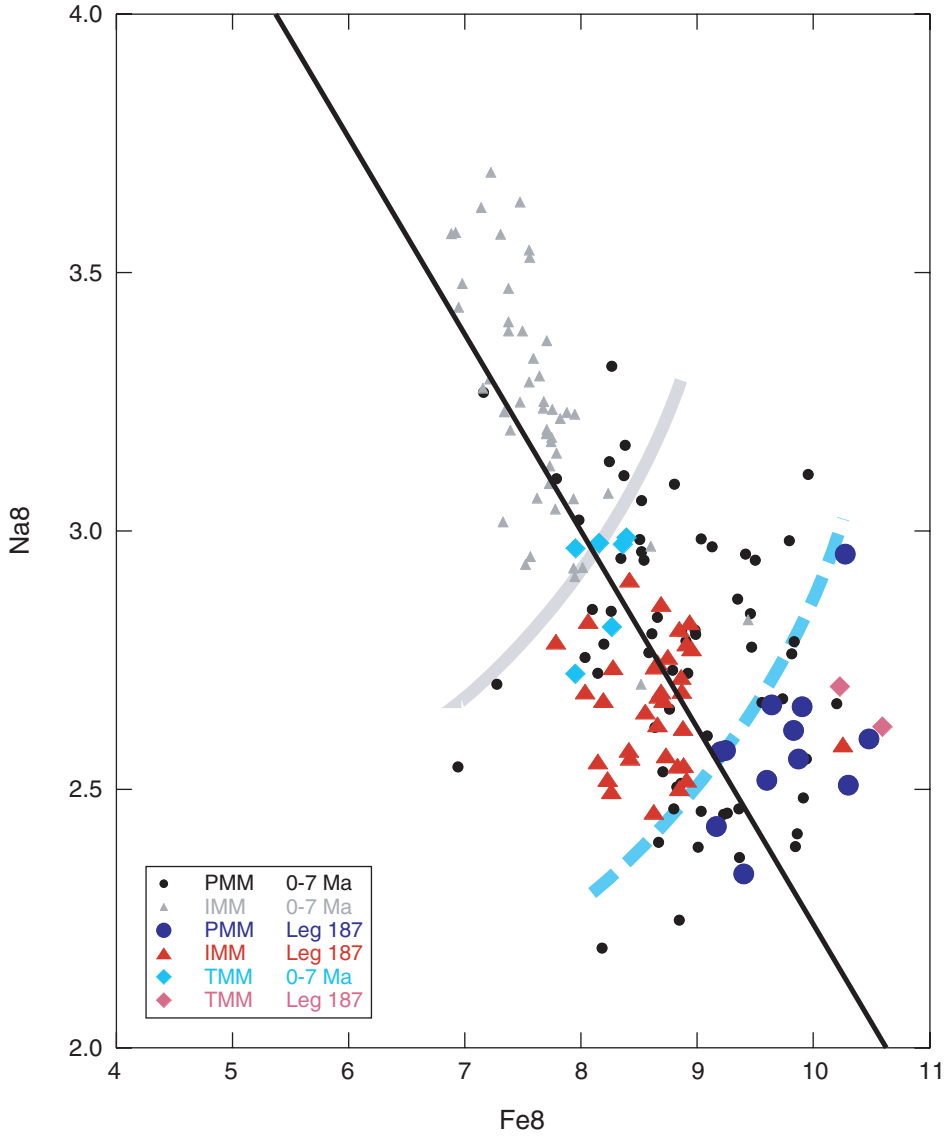

Figure F13. Distribution of εHf values relative to the Indian Ocean MORB mantle (IMM)/Pacific Ocean MORB mantle (PMM) boundary. Note that the boundary for the ODP Leg 187 sites is not exactly co-registered with that for the near-zero–age data. 187 and Vema refer to Leg 187 and dredge data, respectively, of Kempton et al. (2002). 187A refers to Zone A west. Rectangular fields include near-axis data from Hanan et al. (2000a, 2000b, submitted [N1]). TMM = transitional MORB mantle.

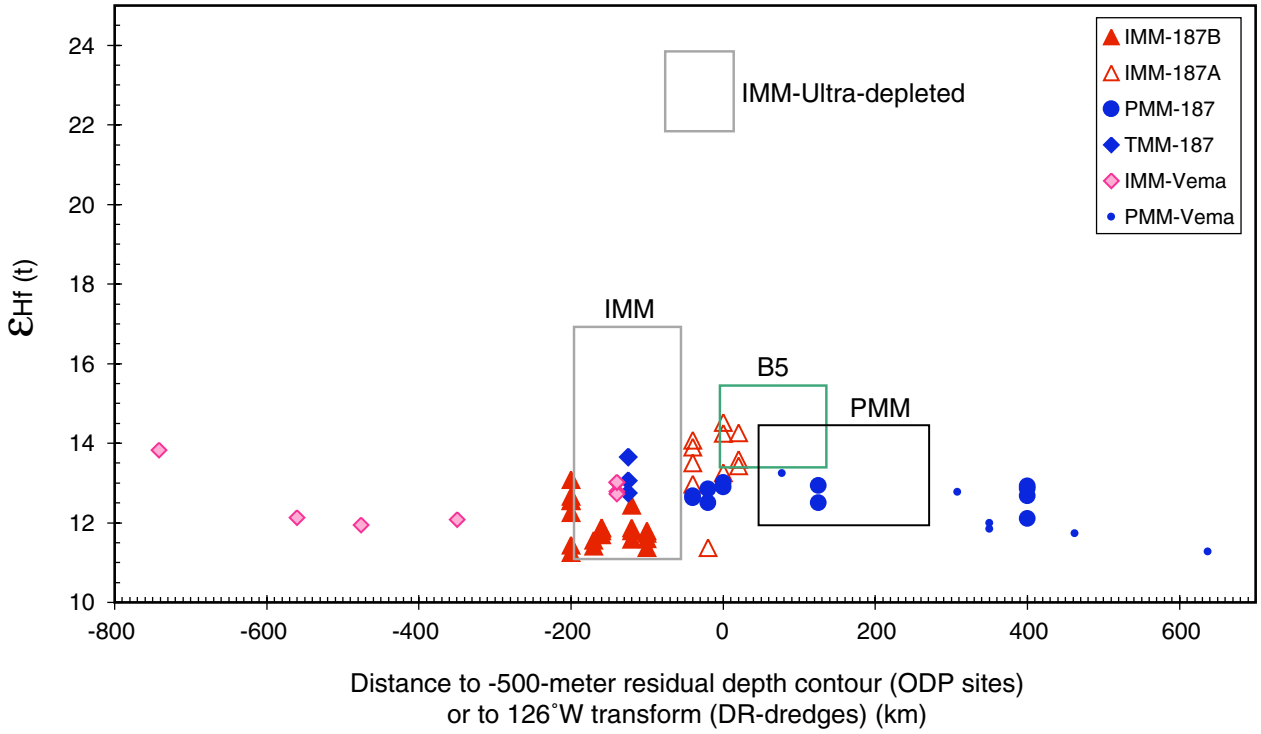

Table T1. Abbreviations and tectonic terminology.

AAD	Australian Antarctic Discordance
AADA	Australian Antarctic depth anomaly
AAMA	Australian Antarctic mantle anomaly
SEIR	Southeast Indian Ridge
Zone A	SEIR east of the AAD
Zone B	SEIR within the AAD
Segment B5	The easternmost transform-bounded axial segment within the AAD. AAD segments are numbered B5 through B1 from east to west.
IMM	Indian (Ocean) MORB mantle (isotopically defined)
PMM	Pacific (Ocean) MORB mantle (isotopically defined)
TMM	Transitional MORB mantle

Note: MORB = mid-ocean-ridge basalt.

CHAPTER NOTES*

N1. Hanan, B.B., Blichert-Toft, J., Pyle, D., and Christie, D.M., submitted. Contrasting origins of the upper mantle MORB source as revealed by Hf and Pb isotopes from the Australian-Antarctic Discordance. *Geochem., Geophys., Geosyst.*

N2. Okino, K., Matsuda, K., Christie, D.M., Nogi, Y., and Koizumi, K., submitted. Development of oceanic detachment and asymmetric spreading at the Australian-Antarctic Discordance. *Geochem., Geophys., Geosyst.*

*Dates reflect file corrections or revisions.